JGR Biogeosciences

RESEARCH ARTICLE
10.1029/2020JG006117

Special Section:
Fire in the Earth System

Delivery of Metals and Dissolved Black Carbon to the Southern California Coastal Ocean via Aerosols and Floodwaters Following the 2017 Thomas Fire

Rachel L. Kelly[1], Xiaopeng Bian[1], Sarah J. Feakins[1], Kyrstin L. Fornace[2], Troy Gunderson[1], Nicholas J. Hawco[1,3], Hengdi Liang[1], Jutta Niggemann[4], Suzanne E. Paulson[5], Paulina Pinedo-Gonzalez[1,6], A. Joshua West[1], Shun-Chung Yang[1], and Seth G. John[1]

[1]Department of Earth Sciences, University of Southern California, Los Angeles, CA, USA, [2]South Coast Air Quality Management District, Diamond Bar, CA, USA, [3]Now at Department of Oceanography, University of Hawai'i at Mānoa, Honolulu, HI, USA, [4]University of Oldenburg, Institute for Chemistry and Biology of the Marine Environment, Oldenburg, Germany, [5]Department of Atmospheric & Oceanic Sciences, University of California Los Angeles, Los Angeles, CA, USA, [6]Now at Lamont-Doherty Earth Observatory of Columbia University, Palisades, NY, USA

Key Points:

- The fire produced large amounts of aerosol metals, including 65, 35, and 5 tons of iron, zinc, and copper, respectively
- Wildfire aerosols transported a larger amount of metals to the coastal ocean versus several days of runoff from the Ventura River
- River water metal concentrations increased on the 37th day of the fire, including iron and lead increases of 61 and 27 times, respectively

Supporting Information:

- Supporting Information S1

Correspondence to:
R. L. Kelly,
kellyrl@usc.edu

Citation:
Kelly, R. L., Bian, X., Feakins, S. J., Fornace, K. L., Gunderson, T., Hawco, N. J., et al. (2021). Delivery of metals and dissolved black carbon to the southern California coastal ocean via aerosols and floodwaters following the 2017 Thomas Fire. *Journal of Geophysical Research: Biogeosciences*, *126*, e2020JG006117. https://doi.org/10.1029/2020JG006117

Received 22 OCT 2020
Accepted 8 JAN 2021

Abstract The Thomas Fire began on December 4, 2017 and burned 281,893 acres over a 40-day period in Ventura and Santa Barbara Counties, making it one of California's most destructive wildfires to date. A major rainstorm then caused a flash flood event, which led to the containment of the fire. Both airborne ash from the fire and the runoff from the flash flood entered into the Santa Barbara Basin (SBB). Here, we present the results from aerosol, river, and seawater studies of black carbon and metal delivery to the SBB associated with the fire and subsequent flash flood. On day 11 of the Thomas Fire, aerosols sampled under the smoke plume were associated with high levels of $PM_{2.5}$, levoglucosan, and black carbon (average: 49 μg/m^3, 1.05 μg/m^3, and 14.93 μg/m^3, respectively) and aerosol metal concentrations were consistent with a forest fire signature. Metal concentrations in SBB surface seawater were higher closer to the coastal perimeter of the fire (including 2.22 nM Fe) than further off the coast, suggesting a dependence on continental proximity rather than fire inputs. On days 37–40 of the fire, before, during, and after the flash flood in the Ventura River, dissolved organic carbon, dissolved black carbon, and dissolved metal concentrations were positively correlated with discharge allowing us to estimate the input of fire products into the coastal ocean. We estimated rapid aerosol delivery during the fire event to be the larger share of fire-derived metal transport compared to runoff from the Ventura River during the flood event.

Plain Language Summary In December 2017, a wildfire on the southern California coast (the Thomas Fire) burned an area almost as large as the city of Los Angeles making it one of California's most destructive wildfires to date. A major rainstorm then began in January 2018, which helped put out the fire and caused a flash flood event. Both ash in the air from the fire and in the water from the flood entered into the coastal ocean. The goal of this study was to observe how the ash in the air and flood waters affected the water chemistry and phytoplankton biomass in the coastal ocean. We sampled the air and seawater in the coastal ocean during the fire and sampled water from the Ventura River, which drains into the ocean, during and after the flood. While both the airborne particulate matter released by the fire and the floodwaters contained high amounts of pollutants, such as metals and soot, we found that these had no major impact on coastal seawater chemistry or phytoplankton biomass. With the increase of wildfires on the western coast of the United States, the importance of studies on how wildfires affect nearby environments, such as the coastal ocean, grows.

1. Introduction

Wildfires have increased in California in recent decades, linked to rising temperatures coinciding with high offshore winds and later onsets of the rainy season (Goss et al., 2020). Extreme fire-inducing conditions in late 2017 led the 2017–2018 Thomas Fire to become the largest wildfire in California's history at the time (Cal Fire, 2018). The Thomas Fire began on December 4, 2017 when two separate fires ignited south of Thomas Aquinas College in Ventura County. Several factors including dry vegetation, unusually strong Santa Ana winds, and low humidity in the winter of 2017 contributed to the spread of the fire. In

2017, California experienced its seventh-wettest year since 1901 (October 1, 2016 through September 30, 2017; USGS, 2020), which promoted the growth of thick grasses and shrubs (Montecito Fire Protection District, 2018). This new vegetation dried out when record-breaking high temperatures were reached in the summer and fall of 2017 (NOAA, 2020; Swain, 2017). The dry vegetation then acted as a fuel for the fire that was spread rapidly by the Santa Ana winds (Montecito Fire Protection District, 2018). Models and observations suggest that the Santa Ana winds were as fast as 32 meters per second at the time of the first ignition, with speeds continuing to increase in the days following (up to 35.3 meters per second; Fovell & Gallagher, 2018). When winds weakened, much of the smoke hung in the air of the affected areas causing the adjacent Santa Barbara County to issue an air quality warning from December 5th through the 29th as the air quality reached unhealthy to hazardous levels ($PM_{2.5}$ concentrations >52.5 $\mu g/m^3$; Santa Barbara County Public Health Department, 2017). The fire lasted for 40 days and burned ~281,893 acres (1,141 km^2) before being 100% contained on January 12, 2018.

A major rainstorm hit Ventura County, Santa Barbara County, and parts of Los Angeles County, starting January 8, 2018, which helped to extinguish the fire. On the morning of January 9 a half-inch of rain fell in 5 min in parts of the Santa Ynez Mountains that had burned during the fire. This intense rain was sufficient to initiate debris flows in the steep-sided fire scars and stream channels (Kean et al., 2019). Enhanced erosion is common in steep landscapes post-fire due to the loss of vegetation that holds topsoil and increases in the soil water repellency (Moody et al., 2013). The debris flows following the Thomas Fire, which occurred mostly near the community of Montecito in Santa Barbara County, damaged 408 residential buildings and caused 23 fatalities (Kean et al., 2019).

The effects from fire-flood sequences, similar to the one associated with the Thomas Fire, extend beyond the initial damage. As both smoke and flood waters from the burned land make their way into the coastal ocean, they carry with them substances released from the burned biomass. These substances include black carbon (BC; e.g., Hunsinger et al., 2008; Olivella et al., 2006; Simoneit & Elias, 2000; Wagner et al., 2018) and trace metals (Burton et al., 2016; Pinedo-Gonzalez et al., 2017; Stein et al., 2012; Young & Jan, 1977 all in Southern California; see Abraham et al., 2017 for a global review). Several studies have explored the ecological and carbon cycle consequences of the pyrogenic chemical influx into terrestrial and freshwater ecosystems (e.g., Charette & Prepas, 2003; Earl & Blinn, 2003; Oliveira-Filho et al., 2018). Fewer studies have focused on the paired fluxes of organics and trace metals to the coastal ocean associated with fires. Trace metal and black carbon fluxes are important, as they can either serve as a nutrient or be toxic to marine organisms. For example, the delivery of a limiting nutrient such as Fe can promote growth (Boyd et al., 2007; Moore et al., 2013), whereas the delivery of Cu (Brand et al., 1983; Paytan et al., 2009), polycyclic aromatic hydrocarbons (PAHs) associated with BC (Campos et al., 2012), or PAHs alongside metals (Brito et al., 2017) can be toxic to marine organisms. As wildfires are projected to increase with warming in the western United States (Abatzoglou & Williams, 2016) understanding their effects on the coastal marine ecosystems will be increasingly important.

A starting point to understanding the effect of wildfires on marine ecosystems is more complete characterization of the transport of black carbon (BC) and metals from fires to the coastal ocean, and documentation of the marine response. Few, if any, studies have considered paired BC and metal loadings, or have evaluated and quantitatively compared both atmospheric and fluvial transport of these substances. With occasional exceptions (e.g., Young & Jan, 1977), little work has connected atmospheric and fluvial measurements with observations of changes in surface seawater composition and the biological response. This study examines aerosols and river runoff associated with the 2017 Thomas Fire to test if fires and related flash flood events significantly affected black carbon and metal delivery to the waters of the Santa Barbara Basin.

2. Materials and Methods

2.1. Field Sampling

On December 14, 2017, day 10 of the Thomas Fire, aerosol and seawater samples were collected from the Santa Barbara Basin aboard a small vessel that departed from Oxnard, California and transected the southern portion of the basin (Figure 1c; Table 1). The Santa Barbara Basin is the northern section of the Southern California Current System (King & Barbeau, 2007; Thunell, 1998), with upwelling of cold salty waters

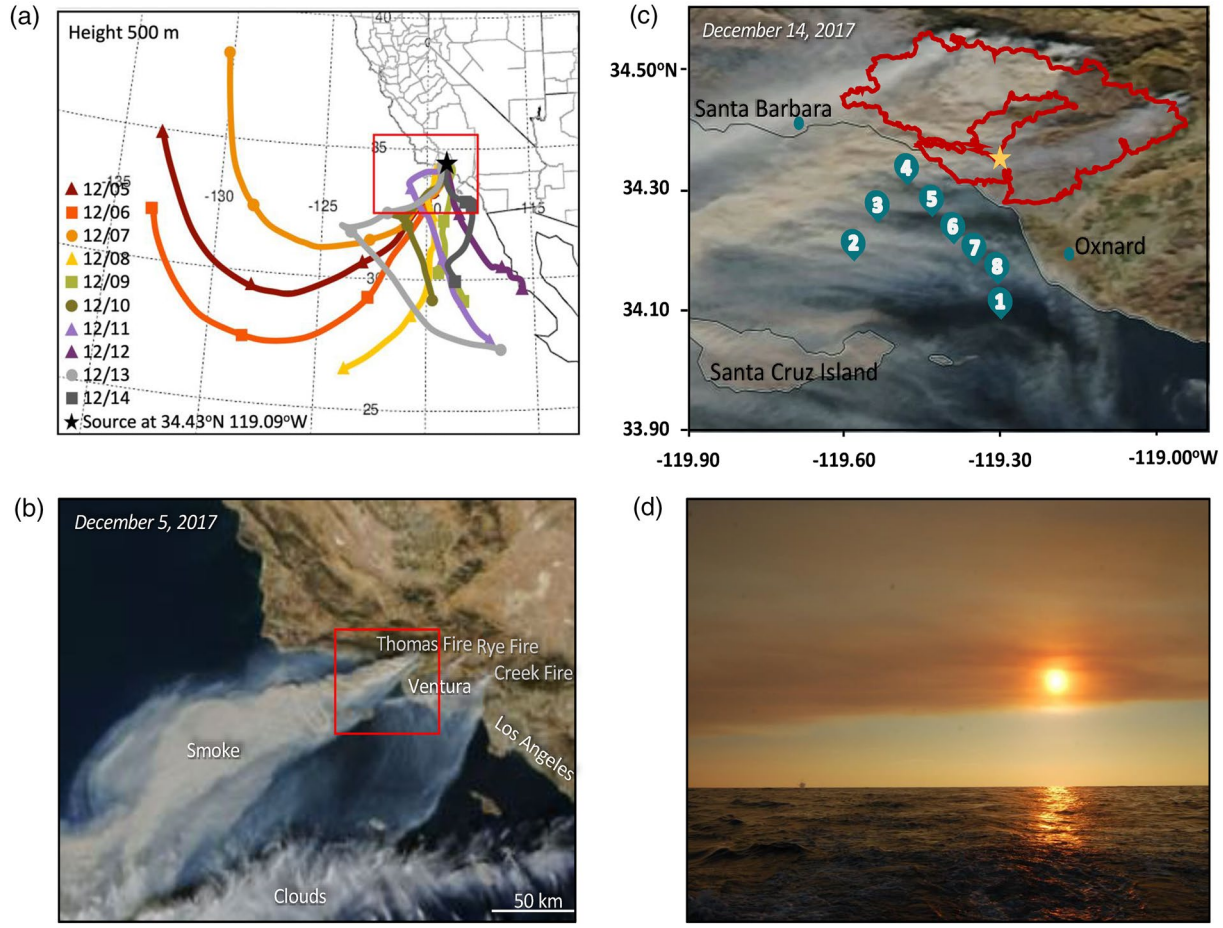

Figure 1. (a) A HYSPLIT model showing the trajectory of the wildfire smoke from December 5–14, 2017 (Rolph et al., 2017; Stein et al., 2015). Red box indicates the area shown in Figure 1B. (b) NASA Earth Observatory image by Joshua Stevens taken on December 5, 2017, the day after the Thomas Fire started. The photo was taken using MODIS data from LANCE/EOSDIS Rapid Response and modified Copernicus Sentinel data processed by the European Space Agency (NASA, 2017b). Red box indicates the area shown in Figure 1C. (c) A satellite image of the Santa Barbara Basin on December 14, 2017, retrieved from NASA worldview, is laid over a map of the basin (NASA, 2017a). Numbered markers represent the stations from the Thomas Fire Cruise conducted as part of this study. The red line shows the perimeter of the Thomas Fire on December 14, 2017 (County of Santa Barbara, 2018). The yellow star is the location where the Ventura River sampling occurred. (d) A photo taken by S. Feakins during the December 14th Thomas Fire Cruise of the smoke plume over the Santa Barbara Basin.

bringing macronutrients to the surface, and relatively high concentrations of chlorophyll *a* and metals (Hayward & Venrick, 1998; Lynn & Simpson, 2008). Primary sources of trace metals to the Santa Barbara Basin include atmospheric deposition, fluvial deposition, upwelling (i.e., the continental shelf and bottom boundary layer), and the equatorward transport of water masses from central California by the California Current system (King & Barbeau, 2011; Thunell, 1998; Warrick et al., 2007). The cruise started ~30 km south of the Thomas Fire at the coast (Station 1) and proceeded northeast to a location directly underneath the smoke plume on the day of sampling (Station 2). The transect then approached the coast closer to the origin of the smoke plume stopping at about 15 and 7 km from the perimeter of the fire (Stations 3 and 4, respectively) and finally returned southeast along the coast toward Oxnard (Stations 5 through 8).

For the aerosol samples, both total suspended particulate (TSP) and particles smaller than 2.5 μm ($PM_{2.5}$) were collected between stations (Table 1). TSP samples were collected on pre-baked quartz fiber filters (QFFs) using two URG© cyclone inlets, and the flow rates were controlled at 33.4 ± 0.1 liters per minute by rotameters (TSI® mass flow meter) (Paulson et al., 2019). $PM_{2.5}$ samples were collected on acid washed, pre-weighed Teflon filters (PALL, 47 mm, 2.5 μm pore size) at 90 ± 2 liters per minute. Samples were collected on average for ~1 h per sample. Two full field blanks were created using the same handling procedures as

Table 1
Samples Taken and Analyses Done During Both Sampling Campaigns of the Thomas Fire in the Santa Barbara Basin and Ventura River

Type	System	Analysis	Materials	Lab
Organic	Aerosol	Levoglucosan	QFF filter	SCAQMD
		Particulate Mass ($PM_{2.5}$)	Teflon filter	UCLA
		Black Carbon	Teflon filter	UCLA
	Marine	Carbon Isotopes	QFF filter	USC
		Chlorophyll *a*	GFF filter	USC
	Marine, River	Dissolved Organic Carbon	SPE-DOC Cartridge	Oldenburg
		Dissolved Black Carbon (BPCA)	SPE-DOC Cartridge	Oldenburg
Trace Metal	Aerosol	Instantaneous Leach	Teflon filter	USC
		Total Digestion	Teflon filter	USC
	Marine, River	Dissolved Concentrations	0.2 μm filtered water	USC
	River	Soluble Concentrations	0.02 μm filtered water	USC
Other	Marine	Nutrients	0.2 μm filtered water	UCSB

samples, but with the pump turned on for only 5 s. After sampling, filters were stored in individual petri dishes in a freezer until analysis.

Surface seawater samples (~2 m depth) were collected using a polytetrafluorethylene (PTFE) Saint Gobain Furon™ bellows pump with low-density polyethylene (LDPE) tubing (Table 1). The inlet tubing was attached to a PVC pole that was positioned in front of the ship. Water was only collected as the vessel steamed into the station to avoid collecting any water that had come into contact with the hull. Samples were filtered in-line with a detachable 0.2 μm polyethersulfone membrane (Pall Acropak™ 1500 capsule filter) and collected in either 50 mL centrifuge tubes or 20 L cubitainers. All sampling materials were soaked in 10% hydrochloric acid and washed extensively with clean water prior to the cruise. Samples were collected following trace metal clean protocols at sea.

Flood water samples were taken from the Ventura River in Foster Park, Ventura from January 8–12, 2018 (Table 1). Sampling started at 5:30 p.m. (PST) on January 8th during a period of low flow before the flood. Flash flooding began at 8:00 a.m. (PST) on January 9th, and sampling proceeded through flooding until January 12th. River samples were collected with a plastic-coated rope and an all-plastic bucket from the center of the stream. The bucket was thrown into the surface of the river, retrieved, and then the contents were poured into both 250 mL bottles (high density polyethylene) and 10 L bags (ethylene vinyl alcohol, food-grade).

2.2. Organic Analyses

2.2.1. Aerosol Samples

Three parameters for organics were measured on the aerosol filters: particulate mass ($PM_{2.5}$), levoglucosan, and black carbon (BC).

2.2.1.1. Particulate Mass ($PM_{2.5}$)

$PM_{2.5}$ is atmospheric particulate matter that has a diameter of <2.5 μm and is used as a proxy for air pollution (Tian et al., 2009). Particulate mass was determined by using a microbalance (1 μg precision, ME 5, Sartorius or similar) to weigh the Teflon filters (11 samples total). Prior to being weighed, the filters were equilibrated at 22°C–24°C and at 42%–44% relative humidity for one hour and were charge neutralized. The blanks had negligible additional mass.

2.2.1.2. Levoglucosan (in TSP)

Levoglucosan (1,6-anhydro-β-D-glucopyranose) is a product of cellulose pyrolysis and a tracer of biomass burning (Simoneit et al., 1999). Six samples for levoglucosan analyses were collected on QFF filters. Levoglucosan was measured with a method adapted from the California Air Resources Board (2014). A portion of each filter was spiked with $^{13}C_6$-levoglucosan (Cambridge Isotope Laboratories) and extracted by ultrasonication in acetonitrile (40°C, 60 min). Extracts were filtered to remove any particles, and an aliquot of each extract was derivatized with Tri-Sil TBT (TMSI:BSA:TMCS, Thermo Fisher Scientific) at 70°C for 60 min. Derivatized extracts were analyzed by GC-MS (Thermo Trace 1310/ISQ LT) using a simultaneous selective ion monitoring (SIM)/full scan method. Levoglucosan was quantified by calibrating mass spectrometry analyses against authenticated levoglucosan standards (Sigma Aldrich, Carbosynth Limited) derivatized in parallel to samples. A method blank (an unexposed filter spiked with ^{13}C-levoglucosan) was also extracted and analyzed to assess any blank contribution to reported results.

2.2.1.3. Black Carbon (in $PM_{2.5}$ and TSP)

Black carbon (BC) is an organic byproduct of the incomplete combustion of organic matter (e.g., fossil fuels, biofuel, and biomass; Ni et al., 2014). In order to measure the amount of black carbon, aerosol filters (11 $PM_{2.5}$ samples and 6 TSP samples) optical absorption at 880 nm was measured using an OT21 dual-wavelength optical transmissometer (Magee Scientific Corporation). Each filter was backed with a quartz diffuser backing (Pallflex Fiberfilm) in order to provide an even distribution of light to the detector (Kuang et al., 2017). Light absorption at 880 nm is proportional to the concentration of elemental carbon, as described by equations presented in Hansen et al. (1984). The term "black carbon" is usually used for material measured optically; elemental carbon is measured chemically, although both types of measurements are operationally defined and should be regarded as estimates. The instrument measures absorption for a reference and sample filter simultaneously and subtracts the reference from the sample. Here, one of the field blank filters was used as the reference.

2.2.2. Surface Seawater Samples

Four parameters for organics were measured on the surface seawater samples: carbon isotopes ($\delta^{13}C$), chlorophyll *a*, dissolved organic carbon (DOC), and dissolved black carbon (DBC).

2.2.2.1. Carbon Isotopes

$\delta^{13}C$ was analyzed to determine the main sources of carbon found in the coastal waters of the Santa Barbara Basin at the time of sampling. Surface seawater particulate samples (8 total) were collected on QFFs for carbon isotope analysis using the identical sample collection and analytical procedures used in Knapp et al. (2016) for $\delta^{15}N$. The QFFs were dried at 60°C and then pelletized in tin capsules before analysis of stable isotopic composition ($\delta^{13}C$) by continuous-flow isotope ratio mass spectrometry. A Costech ECS 4010 elemental analyzer interfaced to a Micromass Isoprime mass spectrometer was used to measure $\delta^{13}C$. Due to varying amounts of material on each filter, 1/8 of a filter was analyzed for each of the filter samples for Stations 1–6, and 1/4 of a filter for Stations 7 and 8. Duplicate filter fractions yielded an average standard deviation of ± 0.20‰. Standards were routinely analyzed during sample runs, which included acetanilide for N and C elemental mass and glycine for $\delta^{13}C$.

2.2.2.2. Chlorophyll a

Chlorophyll *a* was measured to estimate phytoplankton biomass in the surface seawater samples. Surface seawater was collected in 50 mL tubes for chlorophyll *a* analysis. Upon returning to lab, the 8 seawater samples were filtered onto GF/F filters, which were extracted with 90% (V/V) acetone and kept in the dark at −4°C for 24 h (Andersen, 2005). Chlorophyll *a* concentrations were then measured by fluorometry calibrated with a pure chlorophyll *a* standard (Andersen, 2005).

2.2.2.3. Dissolved Organic Carbon and Dissolved Black Carbon

Dissolved organic carbon (DOC) concentrations were quantified on eight frozen filtrate samples (0.7 μm, GFF; filtrate stored in amber glass bottles) after thawing and acidification to pH 2 (HCl, p. a.). Analysis was done using high-temperature combustion on a Shimadzu TOC-VCPH total organic carbon analyzer. Accuracy was monitored by replicate analyses of Deep Atlantic Seawater Reference material (DSR, D.A. Hansell,

University of Miami, Miami, FL), which deviated on average < 5%. Deviation of analytical triplicates of samples was 4 ± 3% on average (range 0%–10%).

Dissolved black carbon (DBC) concentrations were determined following the benzene polycarboxylic acids (BPCA) method (Dittmar et al., 2008), with the modifications described in Stubbins et al. (2012). In brief, aliquots of methanolic solid-phase extracts (Dittmar et al., 2008) were dried, re-dissolved in nitric acid (65%, p. a.) and kept at 170ºC for 9 h. After cooling and evaporation of the acid, the eight samples were dissolved in a phosphate buffer for separation and quantification of benzene polycarboxylic acids on a Waters Acquity UPLC (ultrahigh-performance liquid chromatography) equipped with a photodiode array detector. Concentrations of DBC were calculated from the concentrations of benzene penta- and hexacarboxylic acids based on their power-function relationship (Stubbins et al., 2012). Procedural blanks did not yield any detectable DBC. Half of the samples had enough material to prepare duplicates, three samples were analyzed in quadruplicates and on average replicate analyses deviated 3 ± 2% (range 0%–6%).

2.2.3. River Samples

2.2.3.1. Dissolved Organic Carbon and Dissolved Black Carbon

The analytical methods used for the nine river water samples were the same as applied for "Surface Seawater Samples (Dissolved Organic Carbon and Dissolved Black Carbon)."

2.3. Trace Metal Analyses

All trace metal analyses were performed at the University of Southern California in a class-100 clean room. After preparation of different sample types as described below, final concentrations in all samples were measured on an Element 2 inductively coupled plasma mass spectrometer (ICP-MS, Thermo Fisher Scientific).

2.3.1. Aerosol Samples

Two separate trace metal analyses were done using the Teflon filters: an instantaneous leach and a total digestion. Each analysis was done on a total of 11 aerosol samples.

2.3.1.1. Instantaneous Leach (Soluble Concentrations)

In order to understand the magnitude of aerosol deposition of metals into the ocean and the subsequent dissolution of these metals into the surface waters, we performed instantaneous leaching experiments (Buck et al., 2006). Teflon filters were exposed to ultrapure deionized water for 1 min. The water was collected after exposure and metal concentrations were measured. These metal concentrations were interpreted as the "instantaneous" soluble (i.e., bioavailable) fraction. Each Teflon filter was placed on a 47 mm diameter, Millipore Sterifil Aseptic Filtration System attached to a vacuum pump. 100 mL of Milli-Q water was poured into the filter holder and the filtrate was collected. The filtrate was stored in two 50 mL acid-cleaned centrifuge tubes, which were then acidified to a pH of 2 with distilled HCl and stored for at least one month. The filtration rig was rinsed 3 times with Milli-Q between samples in order to prevent cross-contamination.

436 μL subsamples of the filtrate from the instantaneous leaching experiment were collected and an In standard solution was added to each subsample to achieve a final concentration of 1 ppb In as an internal standard. The samples were then amended with distilled concentrated HNO_3 to achieve a final sample matrix containing 2% HNO_3, followed by ICPMS analysis. Concentrations for all elements were quantified relative to a 10 ppb multielement standard.

2.3.1.2. Total Digestion (Total Concentrations)

Total digestions of the remaining samples were done to measure the total metal concentrations. After the instantaneous leaching, particles on each of the Teflon filters were totally digested in perfluoroalkoxy (PFA) vials using the Piranha digestion method (Ohnemus et al., 2014), except that instead of a three parts concentrated sulfuric acid to one part concentrated hydrogen peroxide solution, a two parts sulfuric acid to one part hydrogen peroxide solution was used. Digested samples were dried down and resuspended with 1 mL 2% HNO_3. 0.1 mL subsamples of the digest were diluted to a final volume of 1 mL with 2% HNO3 which

included 1 ppb In as an internal standard, followed by ICPMS analysis. Concentrations for all elements were quantified relative to a 10 ppb multielement standard.

Total metal concentrations were used to calculate the total mass of metals mobilized through atmospheric transport during the Thomas Fire. First, the amount of burnt biomass produced by the fire was calculated using the following equation:

$$281{,}893\,\text{acres burnt} \times \frac{1\,\text{hectare}}{2.47\,\text{acre}} \times \frac{27\,\text{tons of fuel}}{1\,\text{hectare}} = 3.1 \times 10^6\,\text{tons of burnt biomass} \quad (1)$$

The number of acres burnt and the amount of fuel burned per hectare were values found in Cal Fire (2018) and Van Leeuwen et al. (2014), respectively. Then the amount of pyrogenic aerosols produced was calculated:

$$3.1 \times 10^6\,\text{tons of burnt biomass} \times \frac{1{,}000\,\text{kg}}{1\,\text{ton}} \times \frac{5.46\,\text{g of PM}_{2.5}\,\text{aerosol}}{1\,\text{kg burnt biomass}} = 1.68 \times 10^{10}\,\text{g aerosol} \quad (2)$$

The amount of $PM_{2.5}$ aerosol per amount of burnt biomass is from Hosseini et al. (2013). Finally, the total mass of atmospheric metals was calculated:

$$1.68 \times 10^{10}\ g\,\text{aerosol} \times \frac{1\,\text{metric ton}}{1{,}000{,}000\,\text{g}} \times \frac{x\,\text{TE ppm}}{1{,}000{,}000} = y\,\text{tons of TE in aerosol} \quad (3)$$

where x represents the average concentration of each metal measured in the aerosol samples which is used to calculate y, the total amount of each metal produced by the Thomas Fire.

2.3.2. Surface Seawater Samples

2.3.2.1. Dissolved Concentrations

Filtered (<0.2 μm) surface seawater samples (8 total) were acidified to pH 2 using HCl directly after the cruise and stored for ~2 months. Metal concentration analyses were identical to those used in Hawco et al. (2020). 15 mL subsamples of the filtered seawater were collected and 50 μL of an isotope spike (which includes the following: ^{57}Fe, ^{62}Ni, ^{65}Cu, ^{67}Zn, ^{207}Pb, ^{110}Cd) was added to each of the 15 mL tubes. Spiked samples were then extracted using a seaFAST preconcentration system (manufactured by Elemental Scientific; Lagerström et al., 2013), the instrument pushed each of the samples through a column with Nobias resin PA-1 (Sohrin et al., 2008), and the preconcentrated sample was eluted into 0.5 mL 1 M HNO_3 which included 1 ppb In, followed by ICPMS analysis. Concentrations for all elements except for Mn and Co were derived by using an isotope dilution method (Lee et al., 2011). Mn and Co concentrations were quantified relative to a 10 ppb multielement standard.

2.3.3. River Samples

2.3.3.1. Dissolved and Soluble Concentrations

13 river water samples were first filtered through a 0.2 μm Acropak, subsampled, and then filtered through 0.02 μm Anopore® membrane filters to get the soluble concentrations. 0.1 mL subsamples of the 0.2 and 0.02 μm filtrate were collected and diluted to a final volume of 1 mL with 2% HNO_3 which included 1 ppb In, followed by ICPMS analysis. Concentrations for all elements were quantified relative to a 10 ppb multielement standard.

Both total dissolved (<0.2 μm) and soluble (<0.02 μm) fractions were measured. The colloidal concentrations (0.02–0.2 μm) were calculated by subtracting soluble concentrations from total dissolved concentrations in each sample. Percent soluble and colloidal fractions were then calculated by dividing the respective concentrations by the total dissolved concentrations.

Total dissolved metal concentrations were used to calculate the total mass of metals mobilized through fluvial transport during the January 2018 flash flood event. First, fluvial metal concentrations for each day of the flash flood event were calculated using the equation for the power trendline of the concentration-discharge (C-Q) relationship of each metal in log-log space:

$$y = c \times x^{b} \tag{4}$$

where y is the metal concentration (mol/L), ln(c) is the y-intercept, x is the discharge (m^3/s), and b is the slope of the line. Then using the calculated metal concentration for each day (y) the metal flux was calculated using the following equation:

$$y \times Q \times m_a = j_d \tag{5}$$

where Q is the measured discharge (L/day) for each day from USGS (2020b), m_a is the atomic mass of each metal, and j_d is the daily metal flux (mol/day). The total mass of each metal (metric tons) transported by runoff from January 8 to 12, 2018 was calculated by summing the calculated daily fluxes for each of the 5-days.

2.4. Other Analyses

2.4.1. Nutrients

2.4.1.1. Dissolved Concentrations

About 40 mL of each 0.2 μm filtered, surface seawater sample (8 total) was frozen after collection and sent to the Marine Science Institute at the University of California, Santa Barbara (UCSB) for flow injection analysis. Measurements for phosphate, silicate, ammonia, and nitrite plus nitrate were taken all simultaneously on a QuikChem 8500 Series 2 flow injection analyzer (manufactured by Lachat Instruments). Flow injection analysis (FIA) consisted of a continuously flowing reagent stream, reaction manifolds, and flow-through detectors (Worsfold et al., 2013). Nutrient concentrations were all reported in the micromolar range with a precision of ± 5%.

3. Results

3.1. Organic Analyses

3.1.1. Aerosol Samples

$PM_{2.5}$, levoglucosan, and black carbon concentrations were measured in the aerosol samples. The measured $PM_{2.5}$ values ranged from 33 to 65 μg/m^3 (Figure 2a). The $PM_{2.5}$ concentrations agree well with the offshore projections by the Copernicus Atmosphere Monitoring Service's air quality forecast for December 14, 2017 (the day of the cruise), which ranged from 40 to 70 μg/m^3 (Copernicus Atmosphere Monitoring Service, 2020). The levoglucosan concentrations in the TSP samples ranged from 0.33 to 1.55 μg/m^3 (Figure 2b). The concentrations of BC in the $PM_{2.5}$ ($BC_{PM2.5}$) samples ranged from 5.57 to 16.44 μg/m^3 (Figure 2a) and BC in the TSP (BC_{TSP}) samples ranged from 10.36 to 19.84 μg/m^3 (Figure 2b). $PM_{2.5}$ concentrations generally increased at stations closer to the perimeter of the fire, whereas $BC_{PM2.5}$ concentrations showed no obvious pattern (Figure 2a). In contrast, both levoglucosan (in TSP) and BC_{TSP} concentrations displayed strong trends as both concentrations steadily increased as the cruise approached the coast (Figure 2b). Overall, the highest concentrations for $PM_{2.5,}$ levoglucosan, and BC_{TSP} were all measured near Station 4, the station closest to the perimeter of the fire.

3.1.2. Surface Seawater Samples

The 0.2 μm filtered surface seawater samples were analyzed for both dissolved organic carbon (DOC) and dissolved black carbon (DBC). At the surface of the Santa Barbara Basin, DOC concentrations ranged from 0.392 to 0.846 mM and DBC concentrations ranged from 0.2 to 0.7 μM (Figure S2c). The highest DOC concentration was found at Station 4 (Figure S2c), but no obvious trend was seen in the concentrations at the other 7 stations. Like levoglucosan and BC_{TSP}, DBC concentrations in surface seawater steadily increased as the cruise approached the perimeter of the fire (Figure 2b).

Bulk surface seawater samples were filtered and the particulates were analyzed for both $\delta^{13}C$ and chlorophyll *a*. In the seawater particulates, $\delta^{13}C$ values ranged from −24.50 to −21.14‰ (Figure 2c). Concentrations of

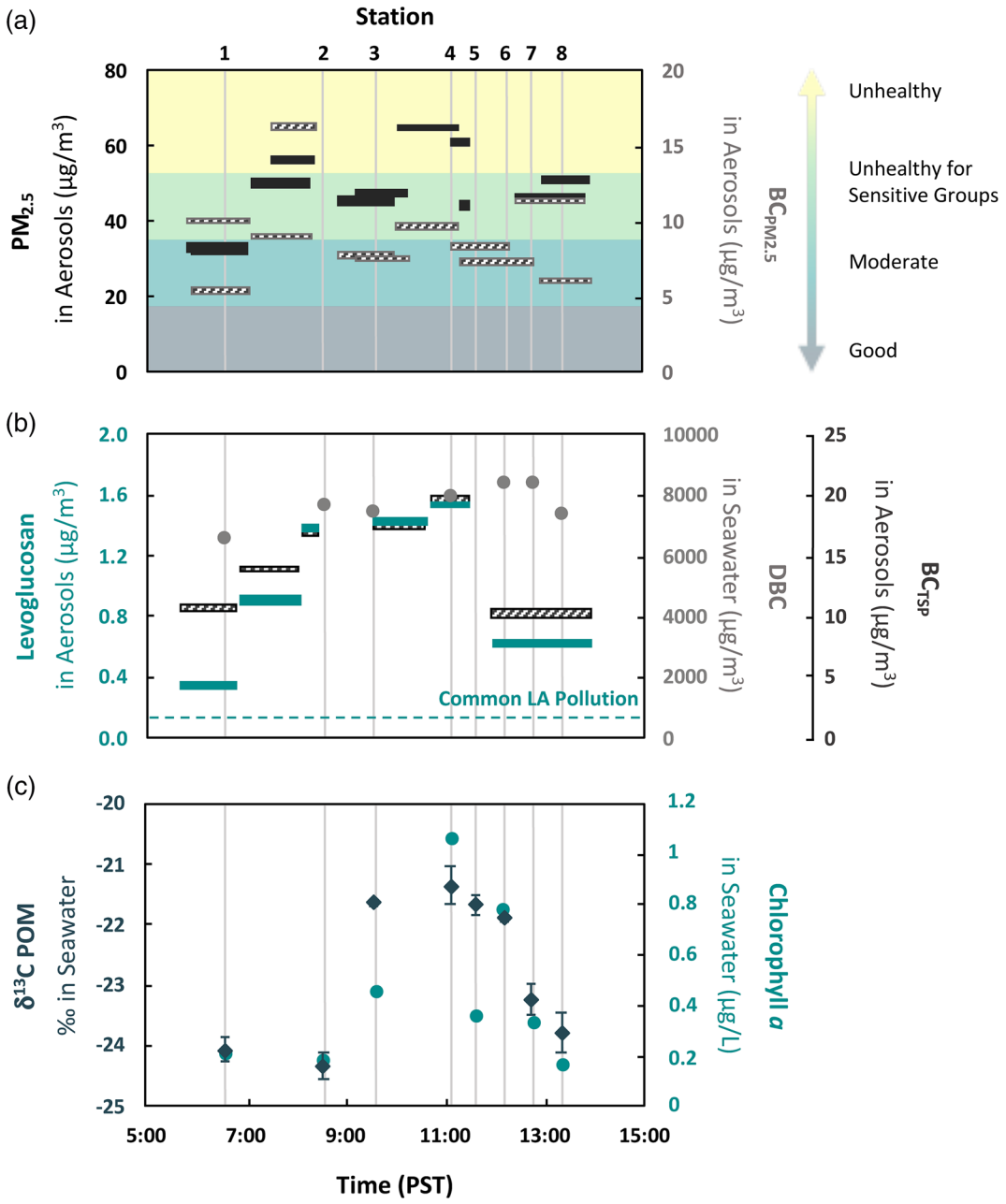

Figure 2. (a) $PM_{2.5}$ concentrations ($\mu g/m^3$) in aerosols are plotted as black rectangles. Black carbon (BC) concentrations ($\mu g/m^3$) in $PM_{2.5}$ are plotted as gray dashed rectangles. Rectangular shaped data points show how long each aerosol sample was collected for. Four categories (good, moderate, unhealthy for sensitive groups, unhealthy) of the United States air quality index (AQI) are shown on the right. (b) Levoglucosan concentrations ($\mu g/m^3$) in aerosols are plotted as teal rectangles. The average levoglucosan concentration found in Central Los Angeles in December 2009 and 2012 is indicated by the dashed line (0.14 ± 0.04 $\mu g/m^3$; Schauer & Sioutas, 2012; Shirmohammadi et al., 2016). Black carbon (BC) concentrations ($\mu g/m^3$) in total suspended particles (TSP) are plotted as black dashed rectangles. Dissolved black carbon (DBC) concentrations ($\mu g/m^3$) in surface seawater are plotted as gray circles. (c) $\delta^{13}C$ values (‰) for particulate organic matter (POM) in surface seawater are plotted as navy blue diamonds. Chlorophyll *a* concentrations ($\mu g/L$) in surface seawater are plotted as teal circles.

chlorophyll *a* ranged from 0.16 to 1.05 μgChla/L (Figure 2c). Both Chl *a* and $\delta^{13}C$ values decreased in the more southern stations (Stations 1, 2, and 8) and increased farther north (Station 4) following the same trend seen in the $PM_{2.5,}$ levoglucosan, BC_{TSP}, and DBC concentrations.

3.1.3. River Samples

River water samples from the Ventura River were analyzed for dissolved organic carbon (DOC) and dissolved black carbon (DBC). DOC concentrations ranged from 181 to 7608 μM and DBC concentrations ranged from 7 to 183 μM (Figure 5c). Concentrations of both DOC and DBC increased along with rising water stage (Figure 5c) and had positive relationships with discharge (Figure S4).

3.2. Trace Metal Analyses

3.2.1. Aerosol Samples

In the aerosol samples, both soluble and total trace metal concentrations were measured. The trace metals analyzed included Fe, Zn, Cd, Ni, Cu, Pb, Mn, and Co. Solubilities decreased in the following order, Zn ≈ Cd > Pb > Mn > Cu > Co > Ni > Fe, which follows a trend found in previous similar studies (Mahowald et al., 2018, Figure 3). Total aerosol metal concentrations are reported as a fraction of the aerosol mass (in ppm; Figure S1), and were also converted into concentrations in the atmosphere ($pmol/m^3$) by normalizing by the total volume of air sampled (Figure 4).

3.2.2. Surface Seawater Samples

Filtered (<0.2 μm) surface seawater samples were measured for dissolved metal concentrations (Fe, Zn, Cd, Ni, Cu, Pb, Mn, and Co; Figure S2a & Table 2). The average metal concentrations of samples taken from all eight stations were 2.42 ± 1.94 nM Fe, 0.88 ± 0.62 nM Zn, 45.90 ± 17.46 pM Cd, 3.07 ± 0.11 nM Ni, 1.16 ± 0.13 nM Cu, 25.35 ± 1.86 pM Pb, 3.06 ± 0.98 nM Mn, and 46.69 ± 13.49 pM Co (Table 2). The lowest concentrations for all of the metals were found at Stations 1 and 8, except for Pb. Surface seawater samples were collected on the 11th day of the fire, and according to NASA worldview satellite images Stations 1 and 8 seem to be the least affected by the smoke produced from the fire in 9 of those previous 11 days (Figure S2). The highest concentrations for all of the metals were found at Stations 3 through 7. Trace metal concentrations follow the same trend found in the organic analyses, where the concentrations increase as the cruise approaches the perimeter of the fire on the coast.

3.2.3. River Samples

In the Ventura River, water samples were taken before, during, and after the January 2018 flash flood event and were analyzed for trace metals (Figure 6). During the flooding, river water dissolved Mn concentrations increased by over two orders of magnitude in comparison to concentrations before the rainstorm. Fe, Pb, and Co concentrations increased at least one order magnitude. Zn and Ni concentrations approximately doubled during flooding. Cu concentrations did not increase by much during flooding, but doubled right after flooding stopped. The metal concentrations in the river water samples increased with rising water stage (Figure 6) and, except for Cd, all had positive relationships with discharge (Figure S4), similar to DOC and DBC concentrations.

3.3. Other Analyses

3.3.1. Nutrients

Nutrient concentrations were measured in the dissolved (<0.2 μM) surface seawater samples (Figure S2b). The average nutrient concentrations in the samples were 0.14 ± 0.06 μM phosphate, 1.49 ± 0.43 μM silicate, 0.69 ± 0.56 μM ammonia, and 0.22 ± 0.24 μM nitrate. These nutrient concentrations are close to the average macronutrient concentrations found in the Santa Barbara Basin during the winter: 0.33 ± 0.12 μM phosphate, 1.75 μM ± 0.7 silicate, 0.19 ± 0.22 μM ammonia, and 0.21 ± 0.18 μM nitrate (data from 2014 to 2018; CalCOFI, 2018). No obvious trend in concentration distribution was seen for any of the nutrients, unlike the organic and metal distributions.

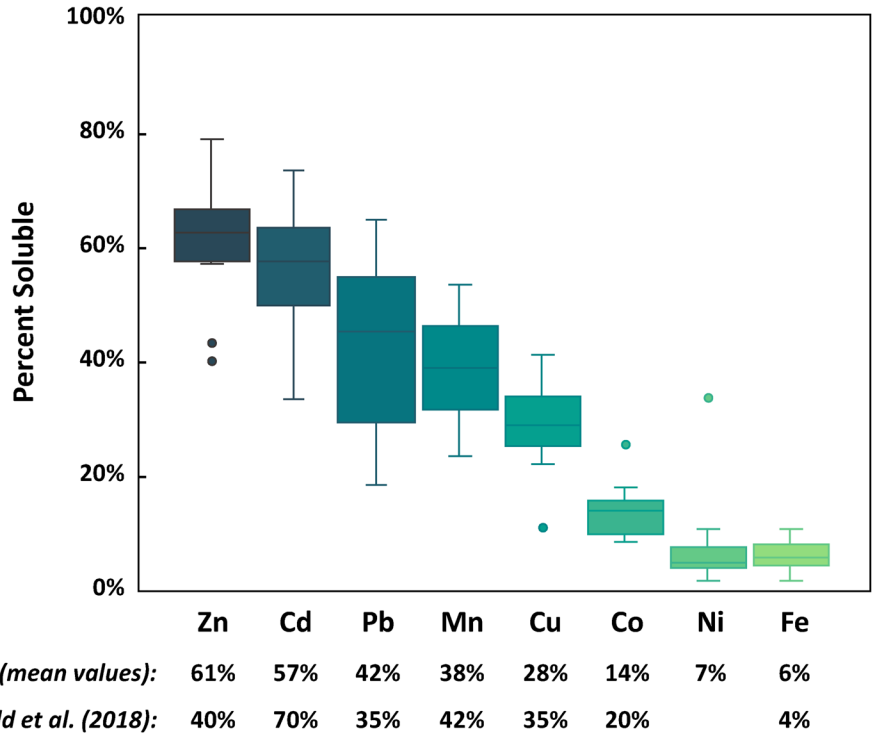

Figure 3. The y-axis shows percentages of the amount of each trace element that was found to be soluble from aerosols collected offshore during the Thomas Fire, following an instantaneous leach experiment (see Methods). The solubility values from this study are compared to values from an aerosol trace metal leaching review by Mahowald et al. (2018). The box plots represent percent soluble values for all 11 aerosol samples for each metal. The lines inside the boxes represent the median (middle value), the lower and upper bounds of the boxes represent the lower and upper quartiles (middle values of the lower and upper halves, respectively), the whiskers represent the minimum and maximum values, and the dots represent outliers.

4. Discussion

4.1. Signatures of Biomass Burning in Aerosols and Delivery of BC to the Surface Ocean

In the aerosol samples we determined the concentrations of multiple parameters which are commonly used as proxies for biomass burning, including $PM_{2.5}$, levoglucosan, and black carbon (Ni et al., 2014; Simoneit et al., 1999, Tian et al., 2009). From 2015 through 2018, the average $PM_{2.5}$ concentration for Ventura and Santa Barbara Counties was 8.4 ± 1.4 μg/m^3 (California Air Resources Board, 2020). During the Thomas Fire, the $PM_{2.5}$ concentrations (33–65 μg/m^3) above the Santa Barbara Basin were 4–8 times higher than the 2015–2018 average and were classified as moderate to unhealthy according to the United States air quality index (AQI; Figure 2a; EPA, 2012). Across the transect, levoglucosan concentrations (0.33–1.55 μg/m^3; Figure 2b) were three orders of magnitude higher than normal, non-fire conditions (0.0012 μg/m^3 in TSP from the California Coast, Fu et al., 2011) (Figure 2b). Similarly, reports from other wildfires found high levoglucosan concentrations (2.70 ± 1.6 μg/m^3) compared to background (during non-fire conditions) reports of 0.06 ± 0.05 μg/m^3 (de Oliveira Alves et al., 2015; Pio et al., 2008; Ward et al., 2006). Additionally, levoglucosan to $PM_{2.5}$ ratios have been shown to vary substantially with fuel types (Hosseini et al., 2013). The average levoglucosan to $PM_{2.5}$ ratio (2.2 ± 1.1 LG/$PM_{2.5}$%) measured on our cruise is close to the results from chaparral test burns (1.64 ± 1.18 LG/$PM_{2.5}$%; Hosseini et al., 2013). Here, our closest sampling station to the perimeter of the fire was ~7 km west of the fire (Station 4, Figure 2) and the plume was visibly higher in the atmosphere than the sea level aerosol sampling (Figure 1d). As we approached the fire, BC concentrations in atmospheric TSP steadily increased together with levoglucosan (from Stations 1 to 4, Figure 2b), which is consistent with wildfires being known as one of the major sources of black carbon to the environment (Kang et al., 2014; Santoso et al., 2013). Atmospheric $PM_{2.5}$ BC sampled during the cruise (5.57–16.44 μg/m^3; Figure 2a) was over three times greater than the annual-average atmospheric $PM_{2.5}$ BC

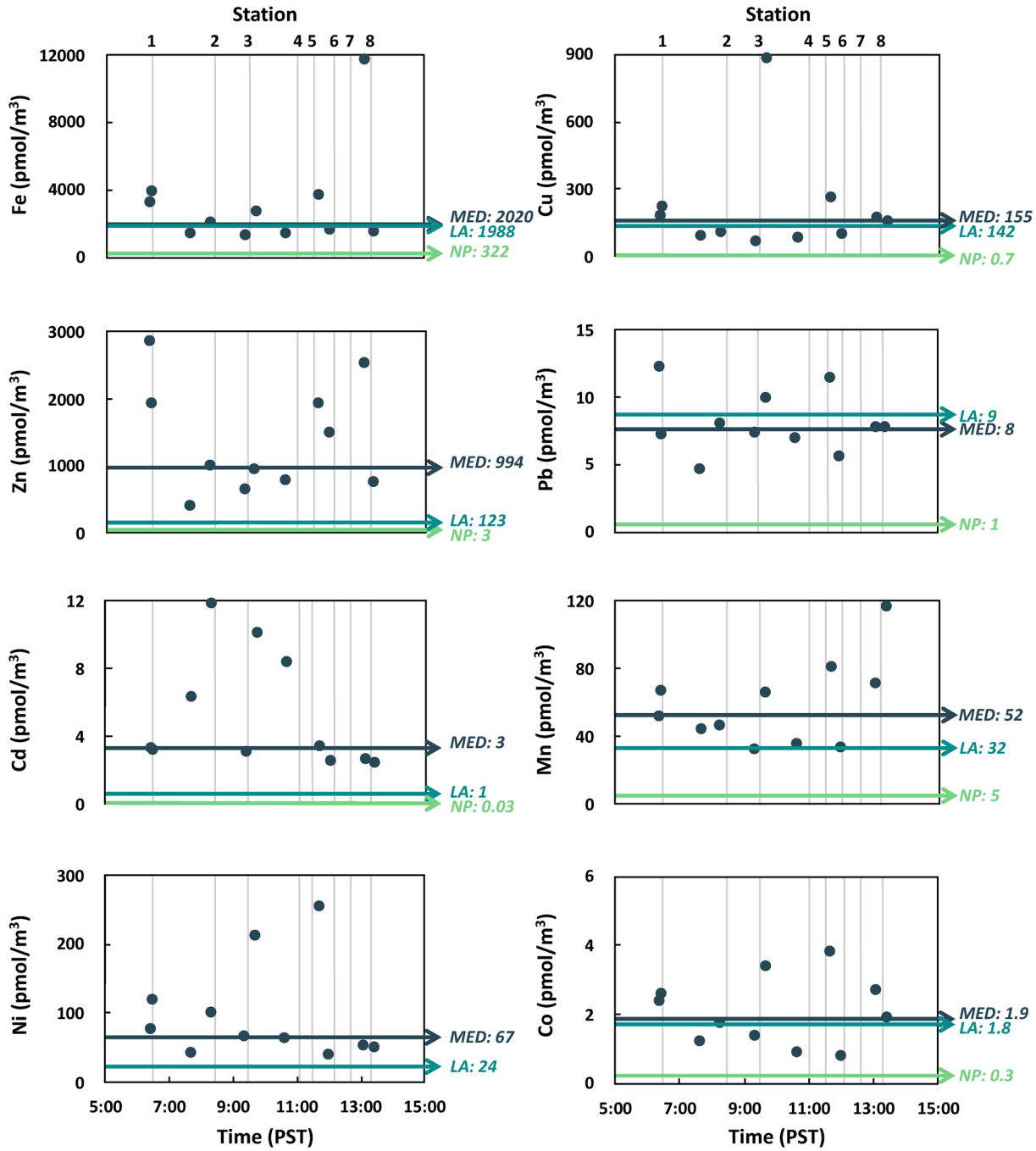

Figure 4. Trace element (TE) load associated with atmospheric aerosols, where $[TE]_{air,PM2.5}$ = (total $PM_{2.5}$ metal quantity)/(total air volume sampled); units are in pmol/m^3. The navy-blue line represents the median (MED) of the concentrations found in this study for aerosols. The green line represents average concentrations for North Pacific aerosols (NP; 11°N and 162°E; Duce et al., 1983). The teal line represents the average for Los Angeles aerosols (LA; Saffari et al., 2013).

found in the Los Angeles Basin from 2003 to 2011 (1.62 μg/m^3, McDonald et al., 2015). The $PM_{2.5}$ BC from this study also exceeded the aerosol BC concentrations reported from three other forest fires, which ranged from 2.4 to 6.04 μg/m^3 (Kang et al., 2014 – Canada; Santoso et al., 2013 – Indonesia). Overall, we found that the aerosol concentrations of $PM_{2.5}$, levoglucosan, and black carbon increased with proximity to the fire under the instantaneous position of the smoke plume.

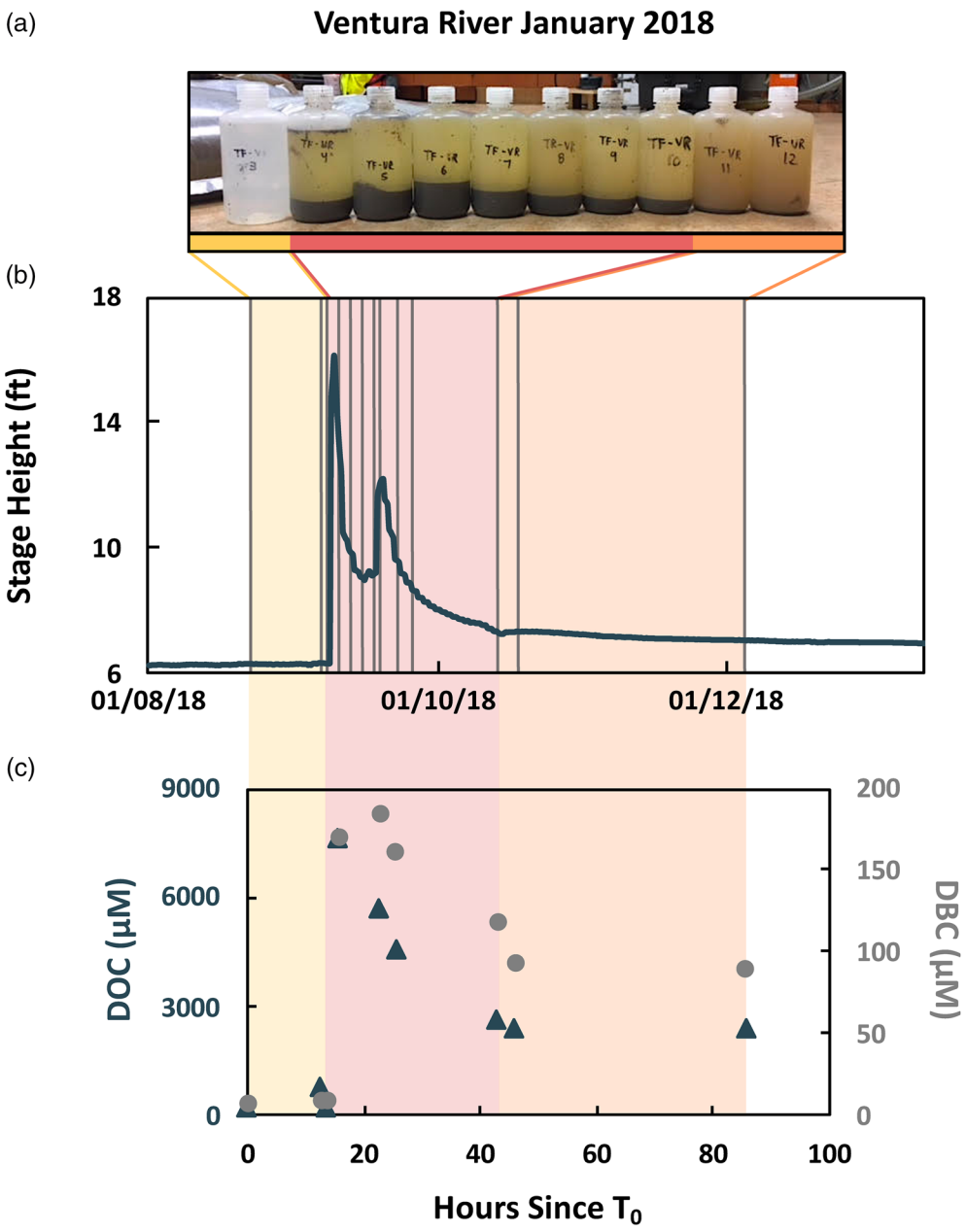

Figure 5. (a) A photo of the trace metal samples taken during river water sampling. (b) The stage height for the Ventura River water before (yellow), during (red), and after (orange) the January 2018 flash flood event (Site 11118500; USGS, 2020b). (c) Dissolved organic carbon concentrations (DOC; μM) in river waters are plotted as navy blue triangles. Dissolved black carbon concentrations (DBC; μM as BPCAs) in river waters are plotted as gray circles. T_0 is the time at which the first sample was taken.

In the surface waters of the Santa Barbara Basin, dissolved black carbon concentrations also increased in waters sampled below the smoke plume (Stations 2 through 7). The slightly elevated DBC in seawater at the stations beneath where aerosol $PM_{2.5}$, levoglucosan, and BC were highest (Figure 2) suggests atmospheric deposition of soluble BC into the basin due to the Thomas Fire. The DBC concentrations in our study (0.55–0.70 μM) were higher than the usual values found in the Pacific open ocean (0.08–0.33 μM; Coppola & Druffel, 2016; Ziolkowski & Druffel, 2010), but were much lower than the minimum values found in other coastal waters, for example, on the coast of the East China Sea (2.58 μM; Wang et al., 2016). Freshly produced BC is thought to be largely insoluble (Wagner et al., 2017), which may explain why the DBC

Table 2
Dissolved Metal Concentration Data for 8 Surface Seawater Samples Collected in the Santa Barbara Basin During the 2017 Thomas Fire

Sample ID	Fe (nM)	Zn (nM)	Cd (pM)	Ni (nM)	Cu (nM)	Pb (pM)	Mn (nM)	Co** (pM)
GSC*	1.45	1.36	413.76	4.19	1.32	26.25	1.49	58.18
Average during the Thomas Fire	2.42±1.94	0.88±0.62	45.90±17.46	3.07±0.11	1.16±0.13	25.35±1.86	3.06±0.98	46.69±13.49
Station 1	0.38	0.15	27.08	2.92	0.97	23.41	2.14	29.55
Station 2	0.43	1.49	30.72	2.97	1.04	24.84	2.17	32.49
Station 3	2.75	1.55	71.49	2.96	1.14	28.32	3.22	50.65
Station 4	2.22	1.75	65.06	3.16	1.30	23.20	5.01	59.42
Station 5	2.61	0.73	61.93	3.19	1.30	27.41	3.64	56.05
Station 6	3.38	0.40	41.45	3.08	1.12	24.25	3.13	45.15
Station 7	6.36	0.51	34.98	3.17	1.31	26.33	3.04	65.72
Station 8	1.23	0.43	34.46	3.11	1.08	25.05	2.11	34.51

*GEOTRACES Surface Coastal (GSC) reference sample collected in the Santa Barbara Basin in 2009 during a period of upwelling. Average of certified values from inter-calibration with other labs.
**Because samples were not UV oxidized, seawater cobalt concentrations do not include the fraction bound by strong organic ligands and therefore resemble 'labile cobalt'.

concentrations at the surface of the Santa Barbara Basin were only slightly elevated. Similarly, a study in Halong Bay, Vietnam found that the atmospheric deposition of BC into the coastal waters did not result in an increase of DBC (Mari et al., 2017). Atmospheric BC becomes soluble through oxidative processes (e.g., weathering, microbial oxidation, photooxidation) that introduce O-containing functional groups (e.g., carboxyl groups), making the molecules more polar (i.e., soluble) (Wagner et al., 2017). Therefore, it is thought that "older" BC is more soluble (Wagner et al., 2017). Since sampling occurred on day 11 of the fire, it is also possible that in the days before sampling any fire-derived DBC in the surface waters may have been removed by adsorption onto sinking particles (Coppola et al., 2014) and/or by photooxidation (Stubbins et al., 2012). Overall, the samples from our study suggest the smoke contributed minimally to the surface seawater DBC inventory at this site. Regardless, we expected that we might see larger atmospheric deposition of soluble metals to these waters from the fire-derived particulates.

4.2. Atmospheric Deposition of Trace Metals into the Santa Barbara Basin

Our sampled aerosol metal concentrations were normalized to the volume of air collected and compared to the average metal concentrations for both North Pacific air (11°N and 162°E; Duce et al., 1983) and Los Angeles air (Saffari et al., 2013) (Figure 4). Except for Pb and Co, the median metal concentrations of the air was at least one order of magnitude higher than the average metal concentrations for the North Pacific and are similar to the average metal concentrations for Los Angeles. Thus, our observations suggest that the Thomas Fire was responsible for elevated metal concentrations observed in the air above the Santa Barbara Basin.

Trace-metal concentrations in our aerosols from the Thomas Fire were compared to those found in wood (Butkus & Baltrėnaitė, 2007; Nicewicz & Szczepkowski, 2008; Queirolo et al., 1990), fly ash from wood burning (Koukouzas et al., 2007; Pitman, 2006; Steenari et al., 1999; Świetlik et al., 2013), ash from two previous California wildfires (Odigie & Flegal, 2011, 2014), and Los Angeles aerosols (Saffari et al., 2013) (Figure S1). The degree of elemental enrichment during burning depends on many factors including the volatility of the elements and the heat of the fire (Bodí et al., 2014). Still, most metal concentrations in aerosols measured here are similar to previously-reported fly ash values; however Fe, Mn, and Pb concentrations were lower than reported fly-ash values, and more similar to concentrations reported for wood.

The relative concentrations and solubility of different trace metals in aerosols is often dependent on the source of the aerosols (i.e., mineral, volcanic, combustion). Aerosols from mineral sources (i.e., dust) are typically enriched with Fe, Mn, Al, and Ti, volcanic aerosols are enriched with Cd, and combustion aerosols

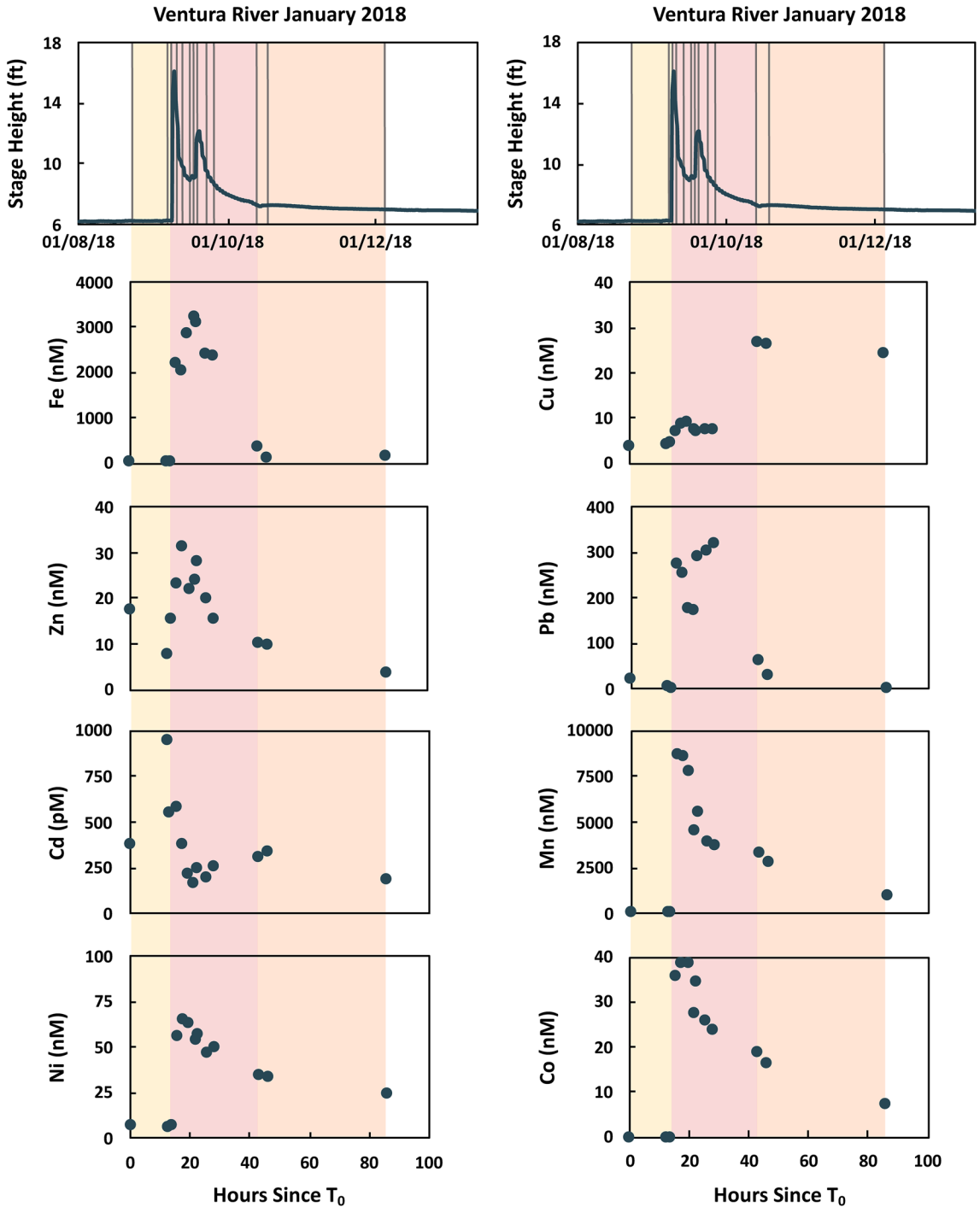

Figure 6. Total dissolved metal concentrations in river samples (<0.2 μm filtrate). Note the changes in ranges of concentrations and changes units on the y-axis of each plot. T_0 is the time at which the first sample was taken.

(i.e., fires) have high concentrations of Zn, Pb, and Cu (Desboeufs et al., 2005; Mahowald et al., 2018). It is therefore not surprising that out of all the metals measured, Zn concentrations in the air were the most elevated compared to samples from non-smoky environments (331 and 8 times greater than North Pacific Ocean and Los Angeles values, respectively) (Figure 4). Metals in aerosols produced from combustion tend to be more soluble than metals associated with dust (Desboeufs et al., 2005; Mahowald et al., 2018; Sedwick et al., 2007). For example, the concentrations of Fe in smoke are 1–2 orders of magnitude lower than in dust

(Mahowald et al., 2018), but Fe associated with biomass burning may be up to 10% more bioavailable than Fe associated with dust (Luo et al., 2008). Therefore, we expected that the Fe and other metals associated with the smoke from the Thomas Fire likely would have a more notable effect on the marine ecosystem than typical dust aerosol deposition.

Evidence of metal deposition into basin waters from smoke aerosols was sought by comparing the trace metal concentrations of the Santa Barbara Basin surface seawater collected from our cruise during the Thomas Fire with a surface seawater sample (GSC reference sample) taken from the basin in 2009 when there was no fire. We found that the metal concentrations during the fire were similar to the background concentrations measured in 2009 (Figure S2a, Table 2). Only Fe and Mn showed higher concentrations during our cruise than in 2009. Average Cd concentrations were almost a whole order of magnitude lower during our cruise than in 2009. However, it is important to note that the GSC reference sample was likely collected during an upwelling event, explaining why the Cd concentration was so high (Segovia-Zavala et al., 1998; Van Geen & Husby, 1996). In any case, the similarity of our data to measurements from 2009 suggests that metals associated with the smoke were not delivered to the surface waters in the Santa Barbara Basin in measurable amounts, or at least that this delivery did not exceed what would be expected from an upwelling event. It is possible that at the time of sampling most of the metals from the Thomas Fire in the surface seawater were still in the particulate size fraction (>0.2 μm), which was not sampled for in this study. Additionally, aerosol flux to the ocean is largely controlled by wet deposition (particularly for finer combustion aerosols; Hand et al., 2004; Zhang et al., 2007) and the sampling in this study took place during a dry period; therefore we might have expected to see a pulse of aerosol deposition when the rain first began in January 2018. The absence of a signal of fire-derived inputs in the dissolved seawater metals is consistent with the lack of dissolved black carbon beneath the smoke plume and with conclusions from prior work on fallout of metals to the oceans after fires in southern California (Young & Jan, 1977).

4.3. Impacts of BC and Metals from Pyrogenic Aerosols on Organisms in the Basin

The Thomas Fire did not appear to have an immediate large impact on organic matter cycling in the Santa Barbara Basin based on $\delta^{13}C$, chlorophyll *a*, or dissolved organic carbon (DOC) concentrations in surface seawater (Figure 2). The highest Chl *a* concentrations were found nearest to the coast, and the measured $\delta^{13}C$ values of seawater particulates were as high as −21.14‰, more consistent with expected values for marine phytoplankton than for terrestrial carbon (Degens, 1969). Away from the fire (Stations 1, 2, and 8; Figure 2c) marine productivity (Chl *a*) declined as $\delta^{13}C$ values decreased to as low as −24.50‰, such that an approximately 50:50 mixture of marine phytoplankton and terrestrial C3 plant inputs (perhaps from the smoke or terrestrial outflow) can be inferred. With the expected increase in trace metal and black carbon fluxes to the coastal ocean due to the fire we expected marine primary productivity to be affected, but the chlorophyll *a* values measured in our samples (0.16–1.05 μg/L) were not significantly different from average Chl *a* values for the Santa Barbara Basin (~1 μg/L; CalCOFI, 2018). Thus, we do not see evidence of a fire-response bloom or bust, and instead the patterns are consistent with normal coastal productivity. In the dissolved organic component, we found no clear relationship between DOC and proximity to the fire, though the DOC concentrations were about six times higher (average: 564 ± 154 μmol/L) than the average values found in the Santa Barbara Basin (~85 μmol/L; Alldredge, 2000; Wear et al., 2015; Figure S2c). These elevated concentrations of DOC might be attributed to atmospheric smoke deposition from the Thomas Fire, perhaps integrated over the 11 previous days of burning; however the elevated DOC cannot be definitively attributed to the Thomas Fire in the absence of elevated DBC, levoglucosan, or other tracers which are diagnostic of biomass burning. Similarly, we cannot attribute the elevated DOC to increased biological productivity stimulated by the Thomas Fire in the absence of elevated macronutrient or trace-metal concentrations. Again, it is possible that the flux of aerosols to the surface waters did not increase until the rainstorm that occurred after sampling in January 2018, in which case we would not have seen an immediate impact on the organic matter in the Santa Barbara Basin due to the Thomas Fire since our sampling took place before these rains.

Although at the time of sampling we found no detectable evidence that the metals associated with the smoke from the Thomas Fire directly impacted the metal inventory of the Santa Barbara Basin, it is possible that the metals in the smoke may have impacted the waters southwest of the basin (beyond where

we collected samples). Based on a satellite image of the smoke plume taken on December 5, 2017 and a HYSPLIT model (Rolph et al., 2017; Stein et al., 2015) showing the trajectory of the wildfire smoke from December 5–14, 2017, the smoke from the fire extended at least ~197 km (Figure 1b) and possibly as much as ~1,000 km (Figure 1a) southwest. Thus the smoke plume extended past the coast through the transition zone of the southern California Current System and into the offshore zone (easternmost reach of the central north Pacific gyre) (King & Barbeau, 2011). The transition zone is characterized as having lower iron concentrations (0.62 ± 0.48 nM Fe) and medium macronutrient concentrations, whereas the offshore zone is characterized as having both low iron (0.18 ± 0.08 nM Fe) and low macronutrient concentrations (King & Barbeau, 2011). If there was any atmospheric deposition of metals from the smoke plume into these waters, the input of soluble metals to both the transition and offshore zones could possibly have stimulated primary production, with those effects being more likely felt in the distant regions beyond the reach of our sampling.

4.4. Increased Loading of Dissolved Metals in River Water after the Thomas Fire

Rivers are another means for transport from burned areas to the oceans. Substantial increases in metal loading to surface waters have been documented after wildfires in southern California (Burton et al., 2016; Stein et al., 2012) and elsewhere (Abraham et al., 2017). These increases have typically been quantified by comparing adjacent catchments, one affected by recent fire and the other not (Burke et al., 2013; Gallaher & Koch, 2004; Pinedo-Gonzalez et al., 2017; Yoon & Stein, 2008). An unburned catchment was not available in this study. Instead, the Ventura River baseflow samples collected before the flash flood event are used to reflect the chemical signature of the river water prior to the fire. This approach assumes there was minimal delivery of fire-associated material to the river prior to rainstorm, which is reasonable if most of the baseflow was from groundwater discharge of "old" water (Hornberger et al., 1998).

Dissolved trace metal concentrations from the Ventura River samples collected before the flooding event (control) and during flooding (burned) were compared to previously-measured metal concentrations in paired catchment studies that looked at runoff from control versus burned landscapes in southern California (Figure S3). The dissolved concentrations of all trace metals measured in this study except Ni were substantially lower compared to those found in other work in southern California (Burke et al., 2013; Gallaher & Koch, 2004; Pinedo-Gonzalez et al., 2017; Yoon & Stein, 2008). This difference may be explained by the location of the Ventura River catchment farther from sources of anthropogenic pollution such as the Los Angeles Basin. Lead concentrations in particular were much lower, which is expected since the primary source of this metal to the ecosystems in this region is anthropogenic aerosols (Odigie & Flegal, 2014). Nonetheless, the data from this study did show increases in river water metal concentrations after the fire-flood event, including for Pb. These findings are consistent with prior studies in Southern California which showed varying degrees of metal enrichment after fires and may be a product of the large increase in river water discharge (pre-flood average: 0.12 ft^3/s vs. flood average: 1,978 ft^3/s) during the rainstorm that followed the Thomas Fire (Figure S3).

The partitioning of the total dissolved trace metal concentrations showed that the colloidal fraction for most of the metals (except Fe and Cu) decreased in the fire-affected conditions ("Flood" and "Post-Flood"; Figure S5a), and conversely that the soluble fraction of these metals increased. These results support the observations made by Pinedo-Gonzalez et al. (2017) in the San Gabriel Mountains that metals in fire-affected runoff may be more soluble (i.e., bioavailable) than metals in non-fire associated runoff. The mechanisms that cause the potential size partitioning of metals due to fires are still unknown, but one proposed mechanism is that the high temperatures during combustion break down organic ligands which could bind metals, resulting in an increase in metal solubility (Gallaher & Koch, 2004).

4.5. Hydrologic Control on Fluvial Mobilization of Trace Metals, DBC, and DOC

Changes in dissolved concentrations as a function of discharge in rivers (concentration-discharge, or C-Q, relationships) can reflect sources and transformation of solutes (e.g., Godsey et al., 2009), as well as revealing how hydrologic conditions influence fluxes to the oceans. In the Ventura River data from this study, the C-Q relationships for DOC and DBC were both positive in log-log space with slopes of 0.29 and 0.32, respectively (Figure S4). These increases in concentration with discharge are consistent with leaching from surface soil

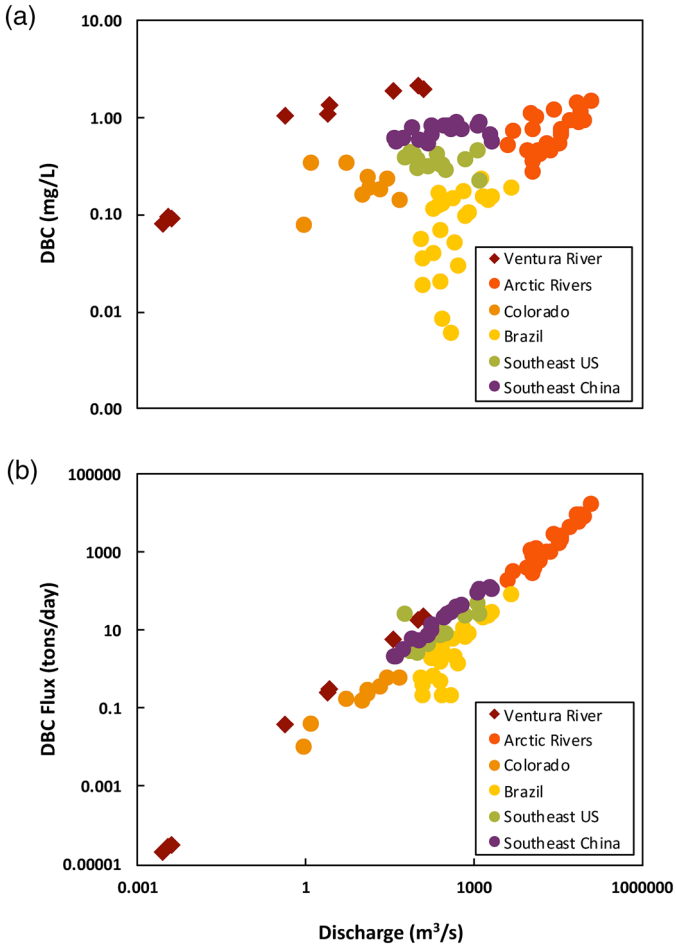

Figure 7. (a) The concentration of dissolved black carbon (DBC) versus discharge (m^3/s) found in this study (Ventura River), the arctic (Myers-Pigg et al., 2017; Stubbins et al., 2012), the Rocky Mountains of Colorado (Wagner et al., 2015), the tropical forests of Brazil (Dittmar et al., 2012), the southeastern US (Roebuck et al., 2018), and southeast China (Bao et al., 2019). (b) Dissolved black carbon (DBC) flux (tons/day) versus discharge (m^3/s).

horizons and may reflect increased flow through these horizons at higher discharge (Lohse et al., 2009; Marques et al., 2017; Perdrial et al., 2014). The positive C-Q relationships seem to reflect a strong hydrological control on the mobilization of DBC and DOC following wildfires: since the flux is a product of water flux multiplied by concentration, positive C-Q relationships magnify the effect of discharge on total export. This effect is well known for DOC (e.g., Raymond et al., 2016). Other studies have shown that most DBC transport also occurs at high discharge, including in tropical forests (Dittmar et al., 2012; Marques et al., 2017), in the arctic (Myers-Pigg et al., 2017; Stubbins et al., 2015), and in the Rocky Mountains of Colorado (Wagner et al., 2015), with a somewhat less pronounced relationship in the southeastern US (Roebuck et al., 2018) and southeast China (Bao et al., 2019) (Figure 7). Here we document this phenomenon in the Mediterranean climate of southern California directly after a wildfire, emphasizing that across a wide variety of climatic regimes, hydrologic conditions are important in determining how much DBC is mobilized from soils and exported in rivers following fires. However, we cannot be certain as to what extent the positive C-Q relationship of DBC and DOC in our study is affected by wildfires due to the lack of DBC and DOC data from the Ventura River in non-fire conditions.

In more detail, when compared to the C-Q relationships for DBC from other studies, the Ventura River samples yield a steeper slope than observed in other regions in the US, but a slightly shallower slope than found for Arctic rivers (Figure 7) – suggesting a relatively strong hydrological control on DBC transport in the Mediterranean climate of southern California compared to other regions. In addition, for a given discharge, DBC concentrations are notably higher in the post-fire Ventura River when compared to other studies. Although this difference may not be surprising since the Ventura River samples were collected immediately after an intense fire in a fire-prone region, the higher concentrations suggest that water-soluble (benzene polycarboxylic acids (BPCA)-derived) DBC can be rapidly eroded in the first rain event after a fire. In contrast, prior studies have found little relationship between the frequency of recent fires and DBC concentrations (Ding et al., 2013; Wagner et al., 2015), perhaps because those studies did not include the initial rapid erosion of fire products, captured here by our rapid-response event sampling.

Many of the metals also showed positive C-Q relationships in the Ventura River, indicating hydrological control on the export of these constituents, too. Again, it is important to note that in this study only one sample was taken post-fire, pre-flood. The positive C-Q slopes for Ni (0.22) and Co (0.26) are similar to those for DOC and DBC, perhaps indicating complexation of these metals with dissolved organic matter, or at least their leaching from similar sources. The log-log C-Q slopes for Cd, Cu, and Zn were all near-zero for the Ventura River, representing "chemostatic behavior" that may reflect minimal leaching from the surface soil layer affected by burning. These elements also showed less enrichment in post-flood versus pre-flood samples compared to the other metals, with especially little enrichment for Cd and Zn, which complements the interpretation of their C-Q relationships that there is less mobilization of these metals from the fire-affected soils. At first glance, the steeper C-Q slopes for Fe (0.44), Pb (0.46), and Mn (0.55) are consistent with their association to colloidal material, which may also be sourced from surface soils and may exhibit steeper C-Q slopes compared to dissolved organics (Trostle et al., 2016). This interpretation is consistent with a study of river water following fire in the San Gabriel Mountains, which found that Fe and Pb were the metals most strongly associated with colloids (Pinedo-Gonzalez et al., 2017; Mn was not reported in that study). However, when considering the colloidal data, there is a rough negative relationship between the C-Q slopes and percent colloidal during the flooding event (Figure S5b). This contradicts the observations made by Trostle et al. (2016), which suggested

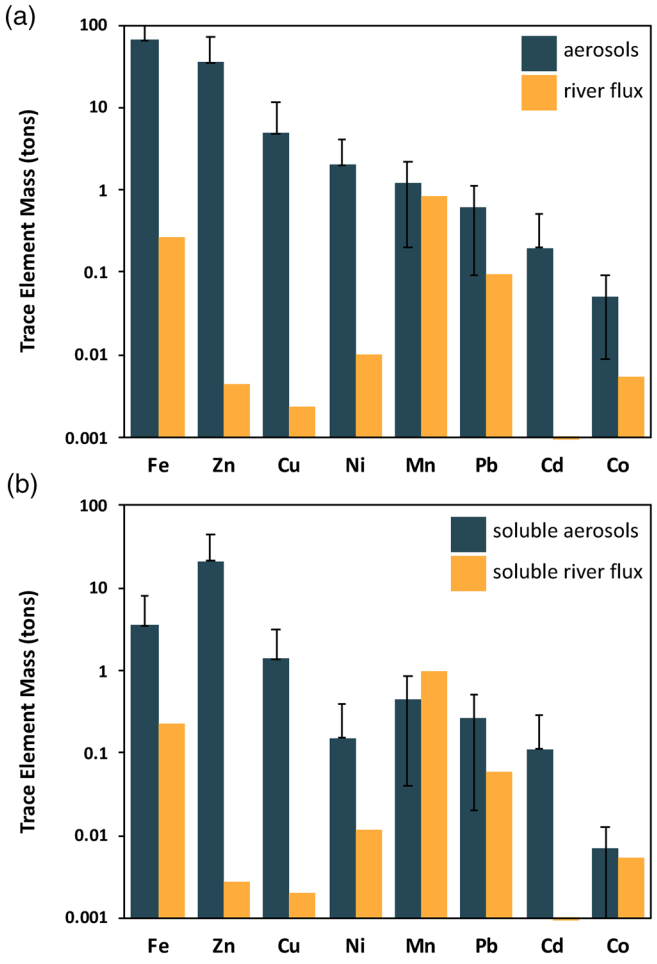

Figure 8. Estimates of the (a) total mass and (b) total soluble mass of each trace metal that was released as aerosols due to the Thomas Fire, and in river flux for the January 8–12, 2018 flash flood event. Some of the Cd estimates not visible due to scale of y-axis.

steeper C-Q slopes are due to greater colloidal association. Our findings thus imply that size partitioning of trace metals may not reflect organic versus non-organic partitioning.

4.6. Fluvial Mobilization of Dissolved Trace Metals and DBC into the Santa Barbara Basin

This study provides data collected over 5 days of the 40-day long Thomas Fire; therefore, in an effort to gauge the full impact of the fire on the Santa Barbara Basin we estimated and compared the total masses of metals brought to the basin and coastal waters further offshore via atmospheric and fluvial transport (Figure 8). The total mass of metals mobilized through atmospheric transport was calculated by multiplying the total amount of burned area from the Thomas Fire (281,893 acres; Cal Fire, 2018) by how much biomass is typically burned for an acre of California chaparral (27 ± 19 tons of fuel per hectare of burnt land; Van Leeuwen et al., 2014) – yielding a total of 3.1×10^6 tons of burnt biomass (Equation 1). Next, the amount of burnt biomass was converted into the amount of particulate matter ($PM_{2.5}$) released, using the amount of $PM_{2.5}$ aerosol per amount of burnt biomass for chaparral fires (5.46 ± 1.31 g $PM_{2.5}$ aerosol per kg of burnt biomass; Hosseini et al., 2013) (Equation 2). This calculation yields a total amount of particulate matter released of 1.68×10^{10} g $PM_{2.5}$ aerosol or 16,825 tons of $PM_{2.5}$ aerosol. The total amount of particulate matter released was then multiplied by the average concentration of each metal measured in aerosols in our samples, to calculate the total amount of each metal produced by the Thomas Fire (Equation 3). We then assume that 100% of the fire-derived $PM_{2.5}$ is deposited into the coastal ocean.

In order to calculate the total mass of metals mobilized through fluvial transport we applied the C-Q relationships to the daily mean discharge values (Q) for the Ventura River (Site 11118500; USGS, 2020b) from January 8, 2018 (start of the rain event) to January 12, 2018. We calculated a metal concentration (C) for each day based on the C-Q relationship and known Q value (Equation 4), then multiplied the calculated C value by Q to get the metal flux for each day (Equation 5). The daily fluxes for each metal were summed over the 5 days of the January storm to calculate the total mass of each metal transported by runoff in the Ventura River during the rain event following the Thomas Fire. We then took into account the fluxes from the larger Santa Clara River (which included some area burned during the Thomas Fire) as well as the smaller mountainous rivers draining along the Santa Barbara coast from burned areas of the Santa Ynez mountains. To account for these areas, we scaled the Ventura River basin fluxes (from a catchment area of 226 square miles) to the entire area burned during the Thomas Fire (440 square miles; yielding a scaling of 1.95 ×). This calculation provides an upper estimate of fluvial fluxes since not all of the Thomas Fire area drains directly to the Santa Barbara Basin.

For Fe, Zn, Cu, Ni, and Cd, we estimate that a larger amount of metal was mobilized by atmospheric transport during the 40-days fire versus 5 days of fluvial transport during the rain event in January 2018. For Mn, Pb, and Co, the atmospheric and fluvial fluxes were not different outside of uncertainty. Only Mn (and perhaps Pb) indicate fluvial fluxes that were higher than atmospheric. In general, then, we expect that the greatest short-term, metal-related impact on the coastal system from the Thomas Fire would have come via the atmospheric pathway. Logistics of coastal sampling during storms meant we were not able to capture coastal seawater composition during the time of the flood runoff, but based on the amount of metals delivered, we have no reason to expect that the effects of the riverine delivery would have been more pronounced than those we observed under the smoke plume during the fire itself. As discussed above, we found those effects to be essentially un-identifiable, except in DBC. However, the atmospheric transport is limited to

the fire event itself, whereas rivers may continue eroding for decades. Previous studies have shown extended increases in sediment/nutrient discharge for years following a fire event (Meixner et al., 2006; Moody et al., 2013; Warrick et al., 2012) due to the lack of terrestrial plants that usually either ground the soil or take up nutrients (Minshall et al., 1989). The long-term flux from rivers would be interesting to ascertain, but was beyond the scope of this study's sampling campaign.

Of all the metals studied, the greatest delivery flux to the coastal ocean was of atmospheric Fe, with ~65 tons delivered to the Santa Barbara Basin and eastern North Pacific as a result of the Thomas Fire. While this input did not appreciably affect Fe concentrations in the Santa Barbara Basin, and in any case the Santa Barbara Basin is not Fe-limited, such a large quantity of Fe could have important biogeochemical consequences if delivered further afield. Applying our measured 5.5% solubility for aerosol Fe suggests 3.5 tons of soluble Fe released from the Thomas Fire. Considering the Fe:C ratios of typical Fe-limited diatoms (~3 μmol Fe per mol C; Marchetti et al., 2006), this Fe could stimulate the production of roughly 250,000 tons of organic carbon. This amount is small compared to total global productivity in HNLC (high-nutrient, low-chlorophyll) regions, and the true stimulation of productivity is likely to be lower because this Fe will not all be delivered to Fe-limited HNLC waters. Nonetheless, this work highlights the potential importance of biomass burning as a globally important source of Fe to the oceans (e.g., Guieu et al., 2005; Matsui et al., 2018). As a fractional share of global aerosol input to the oceans (Jickells, 1995), zinc and copper in the Thomas Fire aerosols seem to have the largest impact representing 0.31% and 0.26% of the annual global input, respectively. Zinc was also the most soluble metal in the Thomas Fire aerosols followed by Cd > Pb > Mn > Cu > Co > Ni > Fe (Figure 3). Iron associated with the Thomas Fire aerosols had a negligible impact on the annual global aerosol input to the oceans, but represents 0.40% of the annual aerosol input into the North Pacific (Buck et al., 2013; Eakins & Sharman, 2010).

5. Conclusion

Black carbon and metals were released by the Thomas Fire and transported by both atmospheric and fluvial pathways to the coastal ocean. For most metals, we estimate that the atmospheric delivery to surface waters was larger than the river transport during the rainstorm after the fire. Although we estimate that substantial amounts of metals were released by the fire, our field measurements of coastal waters from beneath the smoke plume did not reveal metal enrichment which was distinguishable from background concentrations. These results are in accord with prior studies concluding that the direct fallout of metals from the atmosphere after wildfires does not significantly alter southern California coastal ocean metal cycling (Young & Jan, 1977). However, we did observe the signature of black carbon delivery from the smoke plume to the coastal ocean, in terms of elevated dissolved black carbon concentrations in surface waters, but no obvious effect on marine productivity. Our results suggest that the immediate (5-days) fluvial delivery of metals was of a similar or lower magnitude, and therefore also not likely to strongly affect the metal budgets of the coastal system. Nevertheless, we anticipate that fluvial transport may have a longer-term effect on the Santa Barbara Basin as rainfall continues to bring excess sediment and nutrients, potentially along with BC and metals, from the burned coastal watershed many years after the time of the fire (Meixner et al., 2006; Minshall et al., 1989; Moody et al., 2013; Warrick et al., 2012). The extended erosion of sediments and nutrients in watersheds post-wildfire is important because fluvial deposition is one of the major sources of metals to the Santa Barbara Basin, where the residence time of water is < 5 years (Emery, 1960; Krishnaswami et al., 1973; Sholkovitz & Gieskes, 1971). The extended release of sediment into the Santa Barbara Basin means that nutrient and metal inventory of the basin may be affected by the Thomas Fire for years. With the increase in size and frequency of wildfires on the western coast of the United States, but also globally, the importance of studies of the effects of wildfires on nearby ecosystems grows. Our study suggests that research to understand these effects may be most effectively targeted at understanding the long-term fluvial fluxes and their effects on the coastal system, and by studying the far-field effects of metals carried into the open ocean with smoke aerosols.

Data Availability Statement

Research data associated with this article can be accessed in the Open Access Library PANGAEA at https://doi.pangaea.de/10.1594/PANGAEA.926102.

Acknowledgments
This work was funded by the Simons Foundation (SCOPE Award 329108 to John) and the National Science Foundation (NSF-OCE 1736896). The authors also appreciate the contributions from the University of California - Los Angeles, the University of Oldenburg, and the South Coast Air Quality Management District laboratories in providing help with sample collection and analysis. In particular, the authors thank Ina Ulber, Matthias Friebe, and Heike Simon (University of Oldenburg) for technical assistance with DOC and DBC analyses.

References

Abatzoglou, J. T., & Williams, A. P. (2016). Impact of anthropogenic climate change on wildfire across western US forests. *Proceedings of the National Academy of Sciences of the United States of America*, *113*(42), 11770–11775. https://doi.org/10.1073/pnas.1607171113

Abraham, J., Dowling, K., & Florentine, S. (2017). Risk of post-fire metal mobilization into surface water resources: A review. *The Science of the Total Environment*, *599*(600), 1740–1755. https://doi.org/10.1016/j.scitotenv.2017.05.096

Alldredge, A. L. (2000). Interstitial dissolved organic carbon (DOC) concentrations within sinking marine aggregates and their potential contribution to carbon flux. *Limnology & Oceanography*, *45*(6), 1245–1253. https://doi.org/10.4319/lo.2000.45.6.1245

Andersen, R. A. (Ed.), (2005). *Algal culturing techniques*. Elsevier Academic Press. Elsevier.

Bao, H., Niggemann, J., Huang, D., Dittmar, T., & Kao, S. J. (2019). Different responses of dissolved black carbon and dissolved lignin to seasonal hydrological changes and an extreme rain event. *Journal of Geophysical Research: Biogeosciences*, *124*(3), 479–493. https://doi.org/10.1029/2018JG004822

Bodí, M. B., Martin, D. A., Balfour, V. N., Santín, C., Doerr, S. H., Pereira, P., et al. (2014). Wildland fire ash: Production, composition and eco-hydro-geomorphic effects. *Earth-Science Reviews*, *130*, 103–127. http://dx.doi.org/10.1016/j.earscirev.2013.12.007

Boyd, P. W., Jickells, T., Law, C. S., Blain, S., Boyle, E. A., Buesseler, K. O., et al. (2007). Mesoscale Iron Enrichment Experiments 1993-2005: Synthesis and Future Directions. *Science*, *315*(5812), 612–617. https://doi.org/10.1126/science.1131669

Brand, L. E., Sunda, W. G., & Guillard, R. R. L. (1983). Limitation of marine phytoplankton reproductive rates by zinc, manganese, and iron. *Limnology & Oceanography*, *28*(6), 1182–1198. https://doi.org/10.4319/lo.1983.28.6.1182

Brito, D. Q., Passos, C. J. S., Muniz, D. H. F., & Oliveira-Filho, E. C. (2017). Aquatic ecotoxicity of ashes from Brazilian savanna wildfires. *Environmental Science & Pollution Research*, *24*(24), 19671–19682. https://doi.org/10.1007/s11356-017-9578-0

Buck, C. S., Landing, W. M., & Resing, J. (2013). Pacific Ocean aerosols: Deposition and solubility of iron, aluminum, and other trace elements. *Marine Chemistry*, *157*, 117–130. https://doi.org/10.1016/j.marchem.2013.09.005

Buck, C. S., Landing, W. M., Resing, J. A., & Lebon, G. T. (2006). Aerosol iron and aluminum solubility in the northwest Pacific Ocean: Results from the 2002 IOC cruise. *Geochemistry, Geophysics, Geosystems*, *7*(4), 1–21. https://doi.org/10.1029/2005GC000977

Burke, M. P., Hogue, T. S., Kinoshita, A. M., Barco, J., Wessel, C., & Stein, E. D. (2013). Pre- and post-fire pollutant loads in an urban fringe watershed in Southern California. *Environmental Monitoring and Assessment*, *185*(12), 10131–10145. https://doi.org/10.1007/s10661-013-3318-9

Burton, C. A., Hoefen, T. M., Plumlee, G. S., Baumberger, K. L., Backlin, A. R., Gallegos, E., et al. (2016). Trace elements in stormflow, ash, and burned soil following the 2009 station fire in southern California. *PLoS One*, *11*(5), 1–26. https://doi.org/10.1371/journal.pone.0153372

Butkus, D., & Baltrėnaitė, E. (2007). Transport of heavy metals from soil to Pinus sylvestris L. and Betula pendula trees. *Ekologija*, *53*(1), 29–36.

CalCOFI. (2018). *Hydrographic data reports*. Retrieved from https://www.calcofi.org/data/67-hydrographic/450-hydrographic-data-report.html?&modjemcal_id=292&modjemcal_month=5&modjemcal_year=2018

Cal Fire. (2018). *Top 20 most destructive California wildfires, 2019*. Retrieved from http://www.fire.ca.gov/communications/downloads/fact_sheets/Top20_Destruction.pdf

California Air Resources Board. (2014). *Standard operating procedure for the analysis of levoglucosan, mannosan, and galactosan in ambient air samples using gas chromatography/mass spectrometry (SOP MLD073)*. Retrieved from https://ww2.arb.ca.gov/sites/default/files/2020-01/mld073_1.pdf

California Air Resources Board (2020). *iADAM: Air quality data statistics*. Retrieved from https://www.arb.ca.gov/adam/index.html

Campos, I., Abrantes, N., Vidal, T., Bastos, A. C., Gonçalves, F., & Keizer, J. J. (2012). Assessment of the toxicity of ash-loaded runoff from a recently burnt eucalypt plantation. *European Journal of Forest Research*, *131*(6), 1889–1903. https://doi.org/10.1007/s10342-012-0640-7

Charette, T., & Prepas, E. E. (2003). Wildfire impacts on phytoplanktoon communities of three small lakes on the Boreal Plain, Alberta, Canada: a paleolimnological study. *Canadian Journal of Fisheries and Aquatic Sciences*, *60*, 584–593. https://doi.org/10.1139/F03-049

Copernicus Atmosphere Monitoring Service (2020). *Particulate matter forecasts*. Retrieved from https://atmosphere.copernicus.eu/charts/cams/particulate-matter-forecasts?facets=undefined&time=2020081000,3,2020081003&projection=classical_global&layer_name=-composition_pm2p5

Coppola, A. I., & Druffel, E. R. M. (2016). Cycling of black carbon in the ocean. *Geophysical Research Letters*, *43*(9), 4477–4482. https://doi.org/10.1002/2016GL068574

Coppola, A. I., Ziolkowski, L. A., Masiello, C. A., & Druffel, E. R. (2014). Aged black carbon in marine sediments and sinking particles. *Geophysical Research Letters*, *41*(7), 2427–2433. https://doi.org/10.1002/2013GL059068

County of Santa Barbara. (2018). *Thomas fire information and updates*. Retrieved from https://www.countyofsb.org/thomasfire.sbc

Degens, E. T. (1969). Biogeochemistry of Stable Isotopes. In G. Eglinton, & M. T. J. Murphy (Eds.), *Organic geochemistry*. 1st ed. (pp. 304–328). Springer-Verlag Berlin Heidelberg. https://doi.org/10.1038/227634c0

de Oliveira Alves, N., Brito, J., Caumo, S., Arana, A., de Souza Hacon, S., Artaxo, P., et al. (2015). Biomass burning in the Amazon region: Aerosol source apportionment and associated health risk assessment. *Atmospheric Environment*, *120*, 277–285. https://doi.org/10.1016/j.atmosenv.2015.08.059

Desboeufs, K. V., Sofikitis, A., Losno, R., Colin, J. L., & Ausset, P. (2005). Dissolution and solubility of trace metals from natural and anthropogenic aerosol particulate matter. *Chemosphere*, *58*(2), 195–203. https://doi.org/10.1016/j.chemosphere.2004.02.025

Ding, Y., Yamashita, Y., Dodds, W. K., & Jaffé, R. (2013). Dissolved black carbon in grassland streams: Is there an effect of recent fire history?. *Chemosphere*, *90*(10), 2557–2562. https://doi.org/10.1016/j.chemosphere.2012.10.098

Dittmar, T., De Rezende, C. E., Manecki, M., Niggemann, J., Coelho Ovalle, A. R., Stubbins, A., et al. (2012). Continuous flux of dissolved black carbon from a vanished tropical forest biome. *Nature Geoscience*, *5*(9), 618–622. https://doi.org/10.1038/ngeo1541

Dittmar, T., Koch, B., Hertkorn, N., & Kattner, G. (2008). A simple and efficient method for the solid-phase extraction of dissolved organic matter (SPE-DOM) from seawater. *Limnology & Oceanography*, *6*(6), 230–235. https://doi.org/10.4319/lom.2008.6.230

Duce, R. A., Arimoto, R., Ray, B. J., Unni, C. K., & Harder, P. J. (1983). Atmospheric Trace Elements at Enewetak Atoll: 1, Concentrations, Sources, and Temporal Variability. *Journal of Geophysical Research*, *88*(C9), 5321–5342. https://doi.org/10.1029/JC088iC09p05321

Eakins, B. W., & Sharman, G. F. (2010). *Volumes of the world's oceans from ETOPO1*. Boulder, CO: NOAA National Geophysical Data Center.

Earl, S. R., & Blinn, D. W. (2003). Effects of wildfire ash on water chemistry and biota in south-western U.S.A. streams. *Freshwater Biology*, *48*(6), 1015–1030. https://doi.org/10.1046/j.1365-2427.2003.01066.x

Emery, K. O. (1960). *The Sea off southern California, A modern habitat of petroleum*. John Wiley & Sons, Inc. https://doi.org/10.1002/iroh.19610460229

EPA. (2012). *Revised air quality standards for particle pollution and updates to the air quality index (AQI)*.
Fovell, R., & Gallagher, A. (2018). Winds and gusts during the Thomas fire. *Fire*, *1*(3), 47. https://doi.org/10.3390/fire1030047
Fu, P., Kawamura, K., & Miura, K. (2011). Molecular characterization of marine organic aerosols collected during a round-the-world cruise. *Journal of Geophysical Research: Atmospheres*, *116*(13), 1–14. https://doi.org/10.1029/2011JD015604
Gallaher, B. M., & Koch, R. J. (2004). *Cerro grande fire impacts to water quality and stream flow near Los Alamos national laboratory: Results of four years of monitoring*. Retrieved from http://www.lanl.gov/environment/air/docs/cgf/LA-14177.pdf
Godsey, S. E., Kirchner, J. W., & Clow, D. W. (2009). Concentration-discharge relationships reflect chemostatic characteristics of US catchments. *Hydrological Processes*, *23*, 1844–1864. https://doi.org/10.1002/hyp
Goss, M., Swain, D. L., Abatzoglou, J. T., Sarhadi, A., Kolden, C. A., Williams, A. P., et al. (2020). Climate change is increasing the likelihood of extreme autumn wildfire conditions across California. *Environmental Research Letters*, *15*(9), 094016. https://doi.org/10.1088/1748-9326/ab83a7
Guieu, C., Bonnet, S., Wagener, T., & Loÿe-Pilot, M. D. (2005). Biomass burning as a source of dissolved iron to the open ocean?. *Geophysical Research Letters*, *32*(19), 1–5. https://doi.org/10.1029/2005GL022962
Hand, J. L., Mahowald, N. M., Chen, Y., Siefert, R. L., Luo, C., Subramaniam, A., & Fung, I. (2004). Estimates of atmospheric-processed soluble iron from observations and a global mineral aerosol model: Biogeochemical implications. *Journal of Geophysical Research: Atmospheres*, *109*(D17). https://doi.org/10.1029/2004jd004574
Hansen, A. D. A., Rosen, H., & Novakov, T. (1984). The aethalometer - An instrument for the real-time measurement of optical absorption by aerosol particles. *Science of the Total Environment*, *36*, 191–196.
Hawco, N. J., Yang, S. C., Foreman, R. K., Funkey, C. P., Dugenne, M., White, A. E., et al. (2020). Metal isotope signatures from lava-seawater interaction during the 2018 eruption of Kīlauea. *Geochimica et Cosmochimica Acta*, *282*, 340–356. https://doi.org/10.1016/j.gca.2020.05.005
Hayward, T. L., & Venrick, E. L. (1998). Nearsurface pattern in the California Current: coupling between physical and biological structure. *Deep Sea Research Part II: Topical Studies in Oceanography*, *45*, 1617–1638. https://doi.org/10.5565/rev/papers/v40n0.1650
Hornberger, G. M., Raffensperger, J. P., Wiberg, P. L., & Eshleman, K. N. (1998). *Elements of physical hydrology*. Baltimore, MD: John Hopkins University Press.
Hosseini, S., Urbanski, S. P., Dixit, P., Qi, L., Burling, I. R., Yokelson, R. J., et al. (2013). Laboratory characterization of PM emissions from combustion of wildland biomass fuels. *Journal of Geophysical Research: Atmospheres*, *118*(17), 9914–9929. https://doi.org/10.1002/jgrd.50481
Hunsinger, G. B., Mitra, S., Warrick, J. A., & Alexander, C. R. (2008). Oceanic loading of wildfire-derived organic compounds from a small mountainous river. *Journal of Geophysical Research*, *113*(2), 1–14. https://doi.org/10.1029/2007JG000476
Jickells, T. (1995). Atmospheric inputs of metals and nutrients to the oceans: their magnitude and effects. *Marine Chemistry 48*(3–4), 199–214. https://doi.org/10.1016/0304-4203(95)92784-P
Kang, C. M., Gold, D., & Koutrakis, P. (2014). Downwind O3 and PM2.5 speciation during the wildfires in 2002 and 2010. *Atmospheric Environment*, *95*, 511–519. https://doi.org/10.1016/j.atmosenv.2014.07.008
Kean, J. W., Staley, D. M., Lancaster, J. T., Rengers, F. K., Swanson, B. J., Coe, J. A., et al. (2019). Inundation, flow dynamics, and damage in the 9 January 2018 Montecito debris-flow event, California, USA: Opportunities and challenges for post-wildfire risk assessment. *Geosphere*, *15*(4), 1140–1163. https://doi.org/10.1130/GES02048.1
King, A. L., & Barbeau, K. A. (2007). Iron distribution and phytoplankton iron limitation in the southern California Current System. *Marine Ecology Progress Series*, *342*, 91–103.
King, A. L., & Barbeau, K. A. (2011). Dissolved iron and macronutrient distributions in the southern California Current System. *Journal of Geophysical Research: Oceans*, *116*(3), 1–18. https://doi.org/10.1029/2010JC006324
Knapp, A., Casciotti, K., Berelson, W., Prokopenko, M., & Capone, D. (2016). Low rates of nitrogen fixation in eastern tropical South Pacific surface waters. *Proceedings of the National Academy of Sciences of the United States of America*, *113*(16), 4398–4403. https://doi.org/10.1073/pnas.1515641113
Koukouzas, N., Hämäläinen, J., Papanikolaou, D., Tourunen, A., & Jäntti, T. (2007). Mineralogical and elemental composition of fly ash from pilot scale fluidised bed combustion of lignite, bituminous coal, wood chips and their blends. *Fuel*, *86*, 2186–2193. https://doi.org/10.1016/j.fuel.2007.03.036
Krishnaswami, S., Lal, D., Amin, B. S., & Soutar, A. (1973). Geochronological studies in Santa Barbara Basin: 55Fe as a unique tracer for particulate settling. *Limnology & Oceanography*, *18*(5), 763–770. https://doi.org/10.4319/lo.1973.18.5.0763
Kuang, X. M., Scott, J. A., da Rocha, G. O., Betha, R., Price, D. J., Russell, L. M., et al. (2017). Hydroxyl radical formation and soluble trace metal content in particulate matter from renewable diesel and ultra low sulfur diesel in at-sea operations of a research vessel. *Aerosol Science & Technology*, *51*(2), 147–158. https://doi.org/10.1080/02786826.2016.1271938
Lagerström, M. E., Field, M. P., Séguret, M., Fischer, L., Hann, S., & Sherrell, R. M. (2013). Automated on-line flow-injection ICP-MS determination of trace metals (Mn, Fe, Co, Ni, Cu and Zn) in open ocean seawater: Application to the GEOTRACES program. *Marine Chemistry*, *155*, 71–80. https://doi.org/10.1016/j.marchem.2013.06.001
Lee, J. M., Boyle, E. A., Echegoyen-Sanz, Y., Fitzsimmons, J. N., Zhang, R., & Kayser, R. A. (2011). Analysis of trace metals (Cu, Cd, Pb, and Fe) in seawater using single batch nitrilotriacetate resin extraction and isotope dilution inductively coupled plasma mass spectrometry. *Analytica Chimica Acta*, *686*(1–2), 93–101. https://doi.org/10.1016/j.aca.2010.11.052
Lohse, K. A., Brooks, P. D., McIntosh, J. C., Meixner, T., & Huxman, T. E. (2009). Interactions Between Biogeochemistry and Hydrologic Systems. *Annual Review of Environment and Resources*, *34*(1), 65–96. https://doi.org/10.1146/annurev.environ.33.031207.111141
Luo, C., Mahowald, N., Bond, T., Chuang, P. Y., Artaxo, P., Siefert, R., et al. (2008). Combustion iron distribution and deposition. *Global Biogeochemical Cycles*, *22*(1), 1–17. https://doi.org/10.1029/2007GB002964
Lynn, R. J., & Simpson, J. J. (2008). The California current system: The seasonal variability of its physical characteristics. *Journal of Geophysical Research*, *92*(C12), 12947. https://doi.org/10.1029/jc092ic12p12947
Mahowald, N. M., Hamilton, D. S., Mackey, K. R. M., Moore, J. K., Baker, A. R., Scanza, R. A., et al. (2018). Aerosol trace metal leaching and impacts on marine microorganisms. *Nature Communications*, *9*(1). https://doi.org/10.1038/s41467-018-04970-7
Marchetti, A., Maldonado, M. T., Lane, E. S., & Harrison, P. J. (2006). Iron requirements of the pennate diatom Pseudo-nitzschia: Comparison of oceanic (high-nitrate, low-chlorophyll waters) and coastal species. *Limnology & Oceanography*, *51*(5), 2092–2101. https://doi.org/10.4319/lo.2006.51.5.2092
Mari, X., Van, T. C., Guinot, B., Brune, J., Lefebvre, J. P., Raimbault, P., et al. (2017). Seasonal dynamics of atmospheric and river inputs of black carbon, and impacts on biogeochemical cycles in Halong Bay, Vietnam. *Elementa: Science of the Anthropocene*, *5*(75). https://doi.org/10.1525/elementa.255

Marques, J. S. J., Dittmar, T., Niggemann, J., Almeida, M. G., Gomez-Saez, G. V., & Rezende, C. E. (2017). Dissolved black carbon in the headwaters-to-ocean continuum of Paraíba do Sul River, Brazil. *Frontiers of Earth Science*, *5*, 1–12. https://doi.org/10.3389/feart.2017.00011

Matsui, H., Mahowald, N. M., Moteki, N., Hamilton, D. S., Ohata, S., Yoshida, A., et al. (2018). Anthropogenic combustion iron as a complex climate forcer. *Nature Communications*, *9*(1). https://doi.org/10.1038/s41467-018-03997-0

McDonald, B. C., Goldstein, A. H., & Harley, R. A. (2015). Long-term trends in California mobile source emissions and ambient concentrations of black carbon and organic aerosol. *Environmental Science & Technology*, *49*(8), 5178–5188. https://doi.org/10.1021/es505912b

Meixner, T., Fenn, M. E., Wohlgemuth, P., Oxford, M., & Riggan, P. (2006). N saturation symptoms in chaparral catchments are not reversed by prescribed fire. *Environmental Science & Technology*, *40*(9), 2887–2894. https://doi.org/10.1021/es051268z

Minshall, G. W., Brock, J. T., & Varley, J. D. (1989). Wildfires and yellowstone's stream ecosystems. *BioScience*, *39*(10), 707–715. https://doi.org/10.2307/1311002

Montecito Fire Protection District (2018). *A defensible community? A retrospective study of Montecito fire protection district's wildland fire program during the 2017 Thomas fire*. USA: Montecito, CA.

Moody, J. A., Shakesby, R. A., Robichaud, P. R., Cannon, S. H., & Martin, D. A. (2013). Current research issues related to post-wildfire runoff and erosion processes. *Earth-Science Reviews*, *122*, 10–37. https://doi.org/10.1016/j.earscirev.2013.03.004

Moore, C. M., Mills, M. M., Arrigo, K. R., Berman-Frank, I., Bopp, L., Boyd, P. W., et al. (2013). Processes and patterns of oceanic nutrient limitation. *Nature Geoscience*, *6*(9), 701–710. https://doi.org/10.1038/ngeo1765

Myers-Pigg, A. N., Louchouarn, P., & Teisserenc, R. (2017). Flux of dissolved and particulate low-temperature pyrogenic carbon from two high-latitude rivers across the spring freshet hydrograph. *Frontiers in Marine Science*, *4*, 1–11. https://doi.org/10.3389/fmars.2017.00038

NASA. (2017a). In EOSDIS worldview. Retrieved from https://worldview.earthdata.nasa.gov/?v=-148.32622082965645,-24.692629403117117,-25.626600950351538,46.52671342092567

NASA. (2017b). *Smoke and fire in southern California*. Retrieved from https://visibleearth.nasa.gov/images/91379/smoke-and-fire-in-southern-california/91379f

Ni, M., Huang, J., Lu, S., Li, X., Yan, J., & Cen, K. (2014). A review on black carbon emissions, worldwide and in China. *Chemosphere*, *107*, 83–93. https://doi.org/10.1016/j.chemosphere.2014.02.052

Nicewicz, D., & Szczepkowski, A. (2008). The content of heavy metals in the wood of healthy and dying beech trees (Fagus Sylvatica L.) *. *Acta Scientiarum Polonorum Silvarum Colendarum Ratio et Industria Lignaria*, *7*(4), 35–44.

NOAA (2020). *National temperature and precipitation maps*. Retrieved from https://www.ncdc.noaa.gov/temp-and-precip/us-maps/1/201712?products[]=divisionaltavgrank#maps

Odigie, K. O., & Flegal, A. R. (2011). Pyrogenic remobilization of historic industrial lead depositions. *Environmental Science & Technology*, *45*(15), 6290–6295. https://doi.org/10.1021/es200944w

Odigie, K. O., & Flegal, A. R. (2014). Trace metal inventories and lead isotopic composition chronicle a forest fire's remobilization of industrial contaminants deposited in the Angeles National Forest. *PLoS One*, *9*(9). https://doi.org/10.1371/journal.pone.0107835

Ohnemus, D. C., Auro, M. E., Sherrell, R. M., Lagerström, M., Morton, P. L., Twining, B. S., et al. (2014). Laboratory intercomparison of marine particulate digestions including Piranha: A novel chemical method for dissolution of polyethersulfone filters. *Limnology & Oceanography*, *12*, 530–547. https://doi.org/10.4319/lom.2014.12.530

Oliveira-Filho, E. C., Brito, D. Q., Dias, Z. M. B., Guarieiro, M. S., Carvalho, E. L., Fascineli, M. L., et al. (2018). Effects of ashes from a Brazilian Savanna wildfire on water, soil and biota: An ecotoxicological approach. *The Science of the Total Environment*, *618*, 101–111. https://doi.org/10.1016/j.scitotenv.2017.11.051

Olivella, M. A., Ribalta, T. G., De Febrer, A. R., Mollet, J. M., & De Las Heras, F. X. C. (2006). Distribution of polycyclic aromatic hydrocarbons in riverine waters after Mediterranean forest fires. *The Science of the Total Environment*, *355*(1–3), 156–166. https://doi.org/10.1016/j.scitotenv.2005.02.033

Paulson, S. E., Gallimore, P. J., Kuang, X. M., Chen, J. R., Kalberer, M., & Gonzalez, D. H. (2019). A light-driven burst of hydroxyl radicals dominates oxidation chemistry in newly activated cloud droplets. *Science Advances*, *5*(5), 1–8. https://doi.org/10.1126/sciadv.aav7689

Paytan, A., Mackey, K. R. M., Chen, Y., Lima, I. D., Doney, S. C., Mahowald, N., et al. (2009). Toxicity of atmospheric aerosols on marine phytoplankton. *Proceedings of the National Academy of Sciences of the United States of America*, *106*(12), 4601–4605. https://doi.org/10.1073/pnas.0811486106

Perdrial, J. N., McIntosh, J., Harpold, A., Brooks, P. D., Zapata-Rios, X., Ray, J., et al. (2014). Stream water carbon controls in seasonally snow-covered mountain catchments: Impact of inter-annual variability of water fluxes, catchment aspect and seasonal processes. *Biogeochemistry*, *118*(1–3), 273–290. https://doi.org/10.1007/s10533-013-9929-y

Pinedo-Gonzalez, P., Hellige, B., West, A. J., & Sañudo-Wilhelmy, S. A. (2017). Changes in the size partitioning of metals in storm runoff following wildfires: Implications for the transport of bioactive trace metals. *Applied Geochemistry*, *83*, 62–71. https://doi.org/10.1016/j.apgeochem.2016.07.016

Pio, C. A., Legrand, M., Alves, C. A., Oliveira, T., Afonso, J., Caseiro, A., et al. (2008). Chemical composition of atmospheric aerosols during the 2003 summer intense forest fire period. *Atmospheric Environment*, *42*(32), 7530–7543. https://doi.org/10.1016/j.atmosenv.2008.05.032

Pitman, R. M. (2006). Wood ash use in forestry – A review of the environmental impacts. *Forestry*, *79*(5), 563–588. https://doi.org/10.1093/forestry/cpl041

Queirolo, F., Valenta, P., Stegen, S., & Breckle, S. W. (1990). Heavy metal concentrations in oak wood growth rings from the Taunus (Federal Republic of Germany) and the Valdivia (Chile) regions. *Trees*, *4*, 81–87.

Raymond, P. A., Saiers, J. E., & Sobczak, W. V. (2016). Hydrological and biogeochemical controls on watershed dissolved organic matter transport: pulse-shunt concept. *Ecology*, *97*(1), 5–16.

Roebuck, J. A., Medeiros, P. M., Letourneau, M. L., & Jaffé, R. (2018). Hydrological controls on the seasonal variability of dissolved and particulate black carbon in the Altamaha River, GA. *Journal of Geophysical Research: Biogeosciences*, *123*(9), 3055–3071. https://doi.org/10.1029/2018JG004406

Rolph, G., Stein, A., & Stunder, B. (2017). Real-time Environmental Applications and Display sYstem: READY. *Environmental Modelling & Software*, *95*, 210–228. https://doi.org/10.1016/j.envsoft.2017.06.025

Saffari, A., Daher, N., Shafer, M. M., Schauer, J. J., & Sioutas, C. (2013). Seasonal and spatial variation in reactive oxygen species activity of quasi-ultrafine particles (PM0.25) in the Los Angeles metropolitan area and its association with chemical composition. *Atmospheric Environment*, *79*, 566–575. https://doi.org/10.1016/j.atmosenv.2013.07.058

Santa Barbara County Public Health Department (2017). *Air quality watch cancelled for Santa Barbara county*. Retrieved from https://www.countyofsb.org/asset.c/3601

Santoso, M., Dwiana Lestiani, D., & Hopke, P. K. (2013). Atmospheric black carbon in PM2.5 in Indonesian cities. *Journal of Air & Waste Management Association*, *63*(9), 1022–1025. https://doi.org/10.1080/10962247.2013.804465

Schauer, J. J., & Sioutas, C. (2012). *Source apportionment of carbonaceous aerosols using integrated multi-variant and source tracer techniques and a unique molecular marker data set prepared for the California air*. Resources Board and the California Environmental Protection Agency.

Sedwick, P. N., Sholkovitz, E. R., & Church, T. M. (2007). Impact of anthropogenic combustion emissions on the fractional solubility of aerosol iron: Evidence from the Sargasso Sea. *Geochemistry, Geophysics, Geosystems*, *8*(10). https://doi.org/10.1029/2007GC001586

Segovia-Zavala, J. A., Delgadillo-Hinojosa, F., & Alvarez-Borrego, S. (1998). Cadmium in the coastal upwelling area adjacent to the California-Mexico border. *Estuarine, Coastal and Shelf Science*, *46*(4), 475–481. https://doi.org/10.1006/ecss.1997.0296

Shirmohammadi, F., Hasheminassab, S., Saffari, A., Schauer, J. J., Delfino, R. J., & Sioutas, C. (2016). Fine and ultrafine particulate organic carbon in the Los Angeles Basin: Trends in sources and composition. *The Science of the Total Environment*, *541*, 1083–1096. https://doi.org/10.1016/j.scitotenv.2015.09.133

Sholkovitz, E. R., & Gieskes, J. M. (1971). A physical-chemical study of the flushing of the Santa Barbara Basin. *Limnology & Oceanography*, *16*(3), 479–489.

Simoneit, B. R. T., & Elias, V. O. (2000). Organic tracers from biomass burning in atmospheric particulate matter over the ocean. *Marine Chemistry*, *69*(3–4), 301–312. https://doi.org/10.1016/S0304-4203(00)00008-6

Simoneit, B. R. T., Schauer, J. J., Nolte, C. G., Oros, D. R., Elias, V. O., Fraser, M. P., et al. (1999). Levoglucosan, a tracer for cellulose in biomass burning and atmospheric particles. *Atmospheric Environment*, *33*, 173–182. https://doi.org/10.1016/s1352-2310(98)00145-9

Sohrin, Y., Urushihara, S., Nakatsuka, S., Kono, T., Higo, E., Minami, T., et al. (2008). Multielemental determination of GEOTRACES key trace metals in seawater by ICPMS after preconcentration using an ethylenediaminetriacetic acid chelating resin. *Analytical Chemistry*, *80*(16), 6267–6273. https://doi.org/10.1021/ac800500f

Steenari, B. M., Schelander, S., & Lindqvist, O. (1999). Chemical and leaching characteristics of ash from combustion of coal, peat and wood in a 12 MW CFB – A comparative study. *Fuel*, *78*(2), 249–258. https://doi.org/10.1016/S0016-2361(98)00137-9

Stein, A. F., Draxler, R. R., Rolph, G. D., Stunder, B. J. B., Cohen, M. D., & Ngan, F. (2015). NOAA's HYSPLIT Atmospheric Transport and Dispersion Modeling System. *Bulletin of the American Meteorological Society*, *96*(12), 2059–2077. https://doi.org/10.1175/bams-d-14-00110.1

Stein, E. D., Brown, J. S., Hogue, T. S., Burke, M. P., & Kinoshita, A. (2012). Stormwater contaminant loading following southern California wildfires. *Environmental Toxicology & Chemistry*, *31*(11), 2625–2638. https://doi.org/10.1002/etc.1994

Stubbins, A., Niggemann, J., & Dittmar, T. (2012). Photo-lability of deep ocean dissolved black carbon. *Biogeosciences*, *9*(5), 1661–1670. https://doi.org/10.5194/bg-9-1661-2012

Stubbins, A., Spencer, R. G. M., Mann, P. J., Holmes, R. M., McClelland, J. W., Niggemann, J., et al. (2015). Utilizing colored dissolved organic matter to derive dissolved black carbon export by arctic rivers. *Frontiers of Earth Science*, *3*, 1–11. https://doi.org/10.3389/feart.2015.00063

Swain, D. (2017). *2017 hottest summer in California history*. Retrieved from https://www.climatesignals.org/headlines/2017-hottest-summer-california-history

Świetlik, R., Trojanowska, M., & Rabek, P. (2013). Distribution patterns of Cd, Cu, Mn, Pb and Zn in wood fly ash emitted from domestic boilers. *Chemical Speciation and Bioavailability*, *25*(1), 63–70. https://doi.org/10.3184/095422912X13497968675047

Thunell, R. C. (1998). Particle fluxes in a coastal upwelling zone: Sediment trap results from Santa Barbara Basin, California. *Deep Sea Research Part II: Topical Studies in Oceanography*, *45*(8–9), 1863–1884. https://doi.org/10.1016/s0967-0645(98)80020-9

Tian, D., Hu, Y., Wang, Y., Boylan, J. W., Zheng, M., & Russell, A. G. (2009). Assessment of biomass burning emissions and their impacts on urban and regional PM2. 5: A Georgia case study. *Environmental Science & Technology*, *43*(2), 299–305. https://doi.org/10.1021/es801827s

Trostle, K. D., Runyon, J. R., Pohlmann, M. A., Redfield, S. E., Pelletier, J., McIntosh, J., et al. (2016). Colloids and organic matter complexation control trace metal concentration-discharge relationships in Marshall Gulch stream waters. *Water Resources Research*, *52*, 7931–7944. https://doi.org/10.1111/j.1752-1688.1969.tb04897.x

USGS. (2020a). *California drought*. Retrieved from https://ca.water.usgs.gov/california-drought/california-drought-runoff.html

USGS. (2020b). *NWIS site information for USA: Site inventory - Site 11118500*. Retrieved from https://waterdata.usgs.gov/nwis/inventory/?site_no=11118500

Van Geen, A., & Husby, D. M. (1996). Cadmium in the California Current system: Tracer of past and present upwelling. *Journal of Geophysical Research*, *101*(C2), 3489–3507. https://doi.org/10.1029/95JC03302

Van Leeuwen, T. T., Van Der Werf, G. R., Hoffmann, A. A., Detmers, R. G., Rücker, G., French, N. H. F., et al. (2014). Biomass burning fuel consumption rates: A field measurement database. *Biogeosciences*, *11*(24), 7305–7329. https://doi.org/10.5194/bg-11-7305-2014

Wagner, S., Cawley, K. M., Rosario-Ortiz, F. L., & Jaffé, R. (2015). In-stream sources and links between particulate and dissolved black carbon following a wildfire. *Biogeochemistry*, *124*(1–3), 145–161. https://doi.org/10.1007/s10533-015-0088-1

Wagner, S., Ding, Y., & Jaffé, R. (2017). A new perspective on the apparent solubility of dissolved black carbon. *Frontiers of Earth Science*, *5*, 1–16. https://doi.org/10.3389/feart.2017.00075

Wagner, S., Jaffé, R., & Stubbins, A. (2018). Dissolved black carbon in aquatic ecosystems. *Limnology and Oceanography Letter*, *3*(3), 168–185. https://doi.org/10.1002/lol2.10076

Wang, X., Xu, C., Druffel, E. M., Xue, Y., & Qi, Y. (2016). Two black carbon pools transported by the Changjiang and Huanghe Rivers in China. *Global Biogeochemical Cycles*, *30*(12), 1778–1790. https://doi.org/10.1002/2016GB005509

Ward, T. J., Hamilton, R. F., Dixon, R. W., Paulsen, M., & Simpson, C. D. (2006). Characterization and evaluation of smoke tracers in PM: Results from the 2003 Montana wildfire season. *Atmospheric Environment*, *40*(36), 7005–7017. https://doi.org/10.1016/j.atmosenv.2006.06.034

Warrick, J. A., DiGiacomo, P. M., Weisberg, S. B., Nezlin, N. P., Mengel, M., Jones, B. H., et al. (2007). River plume patterns and dynamics within the Southern California Bight. *Continental Shelf Research*, *27*(19), 2427–2448. https://doi.org/10.1016/j.csr.2007.06.015

Warrick, J. A., Hatten, J. A., Pasternack, G. B., Gray, A. B., Goni, M. A., & Wheatcroft, R. A. (2012). The effects of wildfire on the sediment yield of a coastal California watershed. *The Geological Society of America Bulletin*, *124*(7–8), 1130–1146. https://doi.org/10.1130/B30451.1

Wear, E. K., Carlson, C. A., James, A. K., Brzezinski, M. A., Windecker, L. A., & Nelson, C. E. (2015). Synchronous shifts in dissolved organic carbon bioavailability and bacterial community responses over the course of an upwelling-driven phytoplankton bloom. *Limnology & Oceanography*, *60*(2), 657–677. https://doi.org/10.1002/lno.10042

Worsfold, P. J., Clough, R., Lohan, M. C., Monbet, P., Ellis, P. S., Quétel, C. R., et al. (2013). Flow injection analysis as a tool for enhancing oceanographic nutrient measurements—A review. *Analytica Chimica Acta*, *803*, 15–40. https://doi.org/10.1016/j.aca.2013.06.015

Yoon, V. K., & Stein, E. D. (2008). Natural catchments as sources of background levels of storm-water metals, nutrients, and solids. *Journal of Environmental Engineering*, *134*(12), 961–973. https://doi.org/10.1061/(asce)0733-9372(2008)134:12(961)

Young, D. R., & Jan, T. K. (1977). Fire fallout of metals off California. *Marine Pollution Bulletin*, *8*(5), 109–112. https://doi.org/10.1016/0025-326X(77)90133-3

Zhang, G., Zhang, J., & Liu, S. (2007). Characterization of nutrients in the atmospheric wet and dry deposition observed at the two monitoring sites over Yellow Sea and East China Sea. *Journal of Atmospheric Chemistry*, *57*(1), 41–57. https://doi.org/10.1007/s10874-007-9060-3

Ziolkowski, L. A., & Druffel, E. R. M. (2010). Aged black carbon identified in marine dissolved organic carbon. *Geophysical Research Letters*, *37*(16), 4–7. https://doi.org/10.1029/2010GL043963